ACCELERATED IMPLEMENTATION OF INTELLIGENT COMPACTION TECHNOLOGY FOR EMBANKMENT SUBGRADE SOILS, AGGREGATE BASE, AND ASPHALT PAVEMENT MATERIALS

Draft Final Report

Texas DOT FM156 Field Project
July 20 to 25, 2008

Prepared By

David J. White, Ph.D.
Pavana Vennapusa
Heath Gieselman
Luke Johansen
Rachel Goldsmith

Earthworks Engineering Research Center (EERC)
Department of Civil Construction and Environmental Engineering
Iowa State University
2711 South Loop Drive, Suite 4700
Ames, IA 50010-8664
Phone: 515-294-1463
www.ctre.iastate.edu

November 25, 2008

TABLE OF CONTENTS

LIST OF FIGURES

LIST OF TABLES

ACKNOWLEDGMENTS

This study was funded by US FHWA research project DTFH61-07-C-R0032 "Accelerated Implementation of Intelligent Compaction Technology for Embankment Subgrade Soils, Aggregate Base, and Asphalt Pavement Materials". Zhiming Si, Robert L. Graham, and Richard Williammee with TXDOT provide project coordination and assistance with field testing. Stan Allen served as the contractor liaison for Ed Bell Construction Co. Kirby Carpenter from Texana Machinery/Case, Rolland Anderegg with Ammann Compaction Ltd. (Switzerland), and Gert Hanson with Dynapac USA, Inc. provided intelligent compaction rollers and field support during the project. D-SPA tests were conducted by Prof. Soheil Nazarian and Mr. Deren Yuan from the University of Texas at El Paso. George Chang from the Transtec Group, Inc. is the Principal Investigator for this research project. Robert D. Horan is the project facilitator and assisted with scheduling rollers for the project. Many other assisted with the coordination and participated in the field demonstrations and their assistance and interest is greatly appreciated.

INTRODUCTION

The Iowa State University research team conducted field investigations on the FM156 project located in Roanoke, Texas from June 20 – 25, 2008 on Case/Ammann and Dynapac intelligent compaction (IC) rollers. The project involved preparing and testing seven test beds with Type II, III, and V materials (Type II – fine-grained cohesive subgrade clay, Type V – lime stabilized subgrade, and Type III – flex base aggregate material) as identified in the project proposal. Case/Ammann smooth drum and padfoot rollers equipped with roller-integrated stiffness (k_s) and Dynapac smooth drum roller equipped with roller-integrated CMV measurement systems were used on the project. The rollers were equipped with GPS and on-board documentation systems. Goals of this field investigation were to:

- Evaluate the effectiveness of the roller-integrated measurement values (MVs) from padfoot and smooth drum rollers in assessing the compaction quality of three material types (Type II, III and V) encountered on the project,
- Develop correlations between MVs from padfoot and smooth drum rollers and various conventionally used in-situ point measurements in QC/QA practice, and
- Assess comparisons between smooth drum and padfoot roller MVs.

This report presents background information for the two measurement systems evaluated in this study (k_s and CMV), and documents the results and analysis from test bed field studies and the field demonstration activities. Results presented in this report for the padfoot roller are of high priority among many state DOTs and contractor personnel (based on a recent survey conducted by White 2008). To the authors' knowledge, this is the first documented field study to report accelerometer based padfoot roller MVs applications for fine grained cohesive subgrade and lime stabilized subgrade materials, and comparison of padfoot to smooth drum roller MVs. These results should be of significant interest to the pavement, geotechnical, and construction engineering community and are anticipated to promote implementation of compaction monitoring technologies into earthwork construction practice in the United States. Further the results of smooth drum measurements for the Type III flex base aggregate material provided new correlation results.

BACKGROUND

Roller-Integrated Stiffness (k_s) Measurement Value

SV-212 12-ton padfoot and smooth drum Case rollers equipped with Ammann's roller-integrated stiffness k_s measurement value were used on this project (Figure 1). The k_s measurement system was introduced by Ammann during late 1990's considering a lumped parameter two-degree-of-freedom spring dashpot system illustrated in Figure 2 (Anderegg 1998). The spring dashpot model has been found effective in representing the drum-ground interaction behavior (Yoo and Selig 1980). The drum inertia force and eccentric force time histories are determined from drum acceleration and eccentric position (neglecting frame inertia). The drum displacement z_d is determined by double integrating the measured peak drum accelerations. The soil stiffness k_s is determined using Equation 1 when there is no loss of contact between drum

and soil. The k_s value represents a quasi-static stiffness value and is independent of the excitation frequency between 25 to 40 Hz (Anderegg and Kaufmann 2004).

$$k_s = 4\pi^2 f^2 \left(m_d + \frac{m_e r_e \cos(\phi)}{a} \right) \tag{1}$$

where f is the excitation frequency, m_d is the drum mass, $m_e r_e$ is the eccentric moment of the unbalanced mass, φ is the phase angle, a is vibration amplitude. The machines used on this project reported a measurement value approximately every 0.5 m at the drum center along the direction of travel. The k_s measurement system has the capability to perform compaction in a manual mode (i.e., using constant amplitude setting) and in an automatic feedback control (AFC) mode. AFC mode operations, however, were not evaluated at this site.

Figure 1. SV212 padfoot and smooth drum rollers used on the project

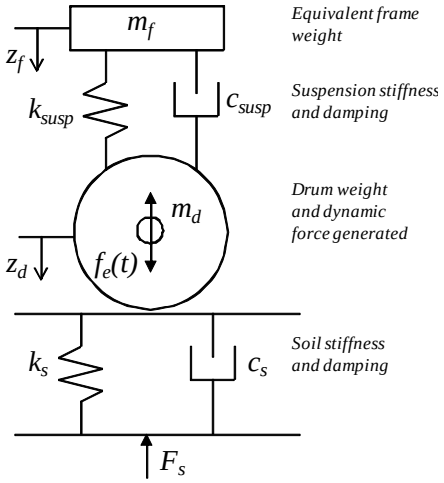

Figure 2. Lumped parameter two-degree-of-freedom spring dashpot model representing vibratory compactor and soil behavior (reproduced from Yoo and Selig 1980)

Prior to initiating the research study, representatives from Case/Ammann conducted a comparison study between the smooth drum and padfoot rollers on different soil types, as use of padfoot rollers was relatively new to this system (Anderegg 2008). The results of the comparison study produced the following conclusions:

1. The ACE system is able to measure the k_s on different types of soils with a smooth drum roller as well using a padfoot roller.
2. Due to higher stresses of a padfoot contact compared to the smooth drum contact over the whole drum, the padfoot roller produce higher k_s values on hard subgrade, i.e., ($k_{s|PD} > k_{s|SD}$) (see Figure 3).
3. The k_s values on soft material, where the padfoot sink into the ground and show a deep footprint, the k_s values are similar for padfoot and smooth drum rollers, i.e., ($k_{s|PD} = k_{s|SD}$) (see Figure 3).
4. The accuracy of the measurement is high for both applications; the significance of the data is equal or higher than similar data measured with a smooth drum.
5. Due to the increased vibrating weight of the padfoot drum, the resonance frequency of the soil-drum-system is decreased. The resulting resonance frequency decreased by about15% due to the added weight of the pad shell.

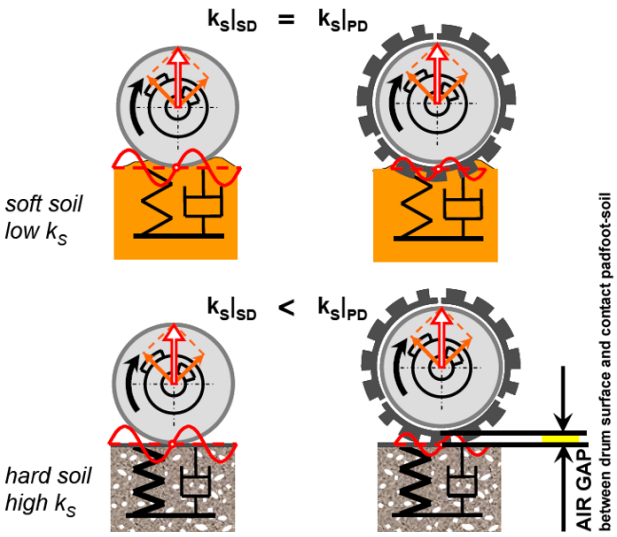

Figure 3. Figure showing the effect of contact footprint on padfoot and smooth drum k_s measurements (Anderegg 2008)

Roller-Integrated Compaction Meter Value (CMV)

A CA-362 15-ton smooth drum roller equipped with the DCA (Dynapac Compaction Analyzer) system was also used on this project (Figure 4). The DCA system measures compaction meter value (CMV) as an indicator of compaction quality. The CMV technology uses accelerometers to measure drum accelerations in response to soil behavior during compaction operations. The ratio between the amplitude of the first harmonic and the amplitude of the fundamental frequency provides an indication of the soil compaction level (Thurner and Sandström, 1980). An increase in CMV indicates increasing compaction. CMV is calculated using Equation 2.

$$CMV = C \cdot \frac{A_1}{A_0} \quad (2)$$

where C = constant, A_1 = acceleration of the first harmonic component of the vibration, and A_0 = acceleration of the fundamental component of the vibration (Sandström & Pettersson, 2004). CMV is a dimensionless parameter that depends on roller dimensions (i.e., drum diameter, weight) and roller operation parameters (i.e., frequency, amplitude, speed). The machine used on this project reported a measurement value approximately every 0.5 m at the drum center along the direction of travel.

The machine also reported a bouncing value (BV) which provides an indication of the drum behavior (e.g., continuous contact, partial uplift, double jump, rocking motion, and chaotic motion) and is calculated using Equation 3, where $A_{0.5}$ = subharmonic acceleration amplitude cause by drum jumping. When the machine is operated in AFC mode, reportedly the amplitude is reduced when BV approaches 14 to prevent drum jumping (personal communication with Gert Hanson, Dynapac). Comparison between AFC mode and manual mode of compaction to assess the effectiveness of AFC on flex base material is presented in this study.

$$BV = C \cdot \frac{A_{0.5}}{A_0} \quad (3)$$

Figure 4. CA-362 smooth drum roller used on the project

EXPERIMENTAL TESTING

Description of Test Beds

A total of seven test beds with three different materials were tested during this field study. A summary of each test bed with material conditions and tests performed is provided in Table 1. A summary of soil index properties for each material is provided in Table 2. Details regarding construction and testing of each test bed are provided in the Appendix.

Table 1. Summary of test beds and in-situ testing

Test Bed	Date	Machine(s)	Drum	Material	Material Type	In-situ Test Measurement
1	7/21/2008	C/A	S, P	Subgrade	II	w, γ_d, CBR, E_{LWD}
2	7/22/2008	C/A, D	S	Flex base and lime stabilized subgrade	III, V	w, γ_d, CBR, E_{LWD}, E_{V1}, E_{V2}, E_{FWD}
3	7/22/2008	C/A	S	Subgrade	II	w, γ_d, E_{LWD}, E_{FWD}, CBR
4	7/23/2008	C/A	S	Flex base	III	(see TB2)
5	7/23/2008	C/A	S, P	Lime stabilized subgrade	V	w, γ_d, CBR, E_{LWD}, E_{V1}/E_{V2}, E_{FWD}
6/7*	7/23/2008	D	S	Flex base	III	w, γ_d, CBR, E_{LWD}, E_{V1}, E_{V2}, E_{FWD}, D-SPA

Note: C/A – Case/Ammann, D – Dynapac, S – Smooth, P – Pad foot, w – moisture content, γ_d – dry unit weight, CBR – California bearing ratio determined from dynamic cone penetrometer (DCP) test, E_{LWD} – elastic modulus determined using light weight deflectometer (LWD), E_{V1} and E_{V2} – initial and reload moduli determined from static plate load test (PLT), E_{FWD} – elastic modulus determined using falling weight deflectometer (FWD) test, D-SPA – dynamic seismic pavement analyzer, *TB 6 involved compaction of flex base material and TB 7 involved performing in-situ point measurements on the compacted layer.

Table 2. Summary of soil index properties

Parameter	Subgrade	Lime Stabilized Subgrade	Flex Base
Material Description (USCS)	Lean clay	Silty sand with gravel	Poorly graded gravel to silty gravel with sand
Gravel Content (%) (> 4.75mm)	3	17	69
Sand Content (%) (4.75mm – 75μm)	10	60	21
Silt Content (%) (75μm – 2μm)	50	19	7
Clay Content (%) (< 2μm)	37	4	3
Coefficient of Uniformity (c_u)	–	71.9	172.9
Coefficient of Curvature (c_c)	–	3.0	14.8
Liquid Limit, LL (%)	41	47	–
Plasticity Index, PI	29	12	–
AASHTO	A-7-6(24)	A-2-7	A-1-a
USCS	CL	SM	GP-GM
Specific Gravity, G_s (assumed)	2.65	2.65	2.65

In-situ Testing Methods

Six different in-situ testing methods were employed in this study to evaluate the in-situ soil physical and mechanical properties (Figure 5): (a) 200-mm diameter Zorn LWD setup with 50 mm drop height to determine elastic modulus ($E_{LWD\text{-}Z2}$), (b) Dynamic Cone Penetrometer (DCP) to determine California bearing Ratio (CBR), (c) calibrated nuclear moisture-density gauge (NG), (d) 300-mm diameter Dynatest FWD to determine elastic modulus (E_{FWD}), (e) 300-mm diameter static PLT to determine initial (E_{V1}) and re-load modulus (E_{V2}), and (f) D-SPA to determine low-strain elastic modulus ($E_{D\text{-}SPA}$). LWD, DCP, NG, and PLT tests were conducted by the ISU research team with aid of the geotechnical mobile lab (Figure 5g), FWD tests were conducted by TXDOT personnel (Mr. Robert L. Graham), and D-SPA tests were conducted by University of Texas at El Paso personnel (Prof. Soheil Nazarian and Mr. Deren Yuan).

LWD tests were performed following manufacturer recommendations (Zorn 2003) and the $E_{LWD\text{-}Z2}$ value was determined using Equation 4, where E = elastic modulus (MPa), d_0 = measured settlement (mm), v = Poisson's ratio, σ_0 = applied stress (MPa), r = radius of the plate (mm), f = shape factor depending on stress distribution (assumed as 8/3 for flex base and $\pi/2$ for subgrade and lime stabilized subgrade materials). When padfoot roller was used for compaction, the material was carefully excavated down to the bottom of the pad to create a level surface for LWD testing.

$$E = \frac{(1-v^2)\sigma_0 r}{d_0} \times f \tag{4}$$

DCP test was performed in accordance with ASTM D6951-03 to determine dynamic cone penetration index (DPI) and calculate CBR using Equation 5. The DCP test results are presented in this report as CBR point values or CBR profiles. When the data is presented as point values, the data represents an average CBR of the compaction layer or the depth specified (e.g., $CBR_{0\text{-}250}$ represents 0-250 mm depth).

$$CBR = \frac{292}{DPI^{1.12}} \tag{5}$$

$E_{FWD\text{-}D3}$ values were determined from the stiffness values using Equation 4 (f values were assumed as stated above). Static PLT's were conducted by applying a static load on 300 mm diameter plate against a 6.2kN capacity reaction force. The applied load was measured using a 90-kN load cell and deformations were measured using three 50-mm linear voltage displacement transducers (LVDTs). The load and deformation readings were continuously recorded during the test using a data logger. The E_{V1} and E_{V2} values were determined from Equation 4, using appropriate stress and deflection values as illustrated in Figure 5 depending on the material/layer type. The D-SPA test developed by Nazarian et al. (1993) was used on the project. The resulting modulus values were provided from Transtec.

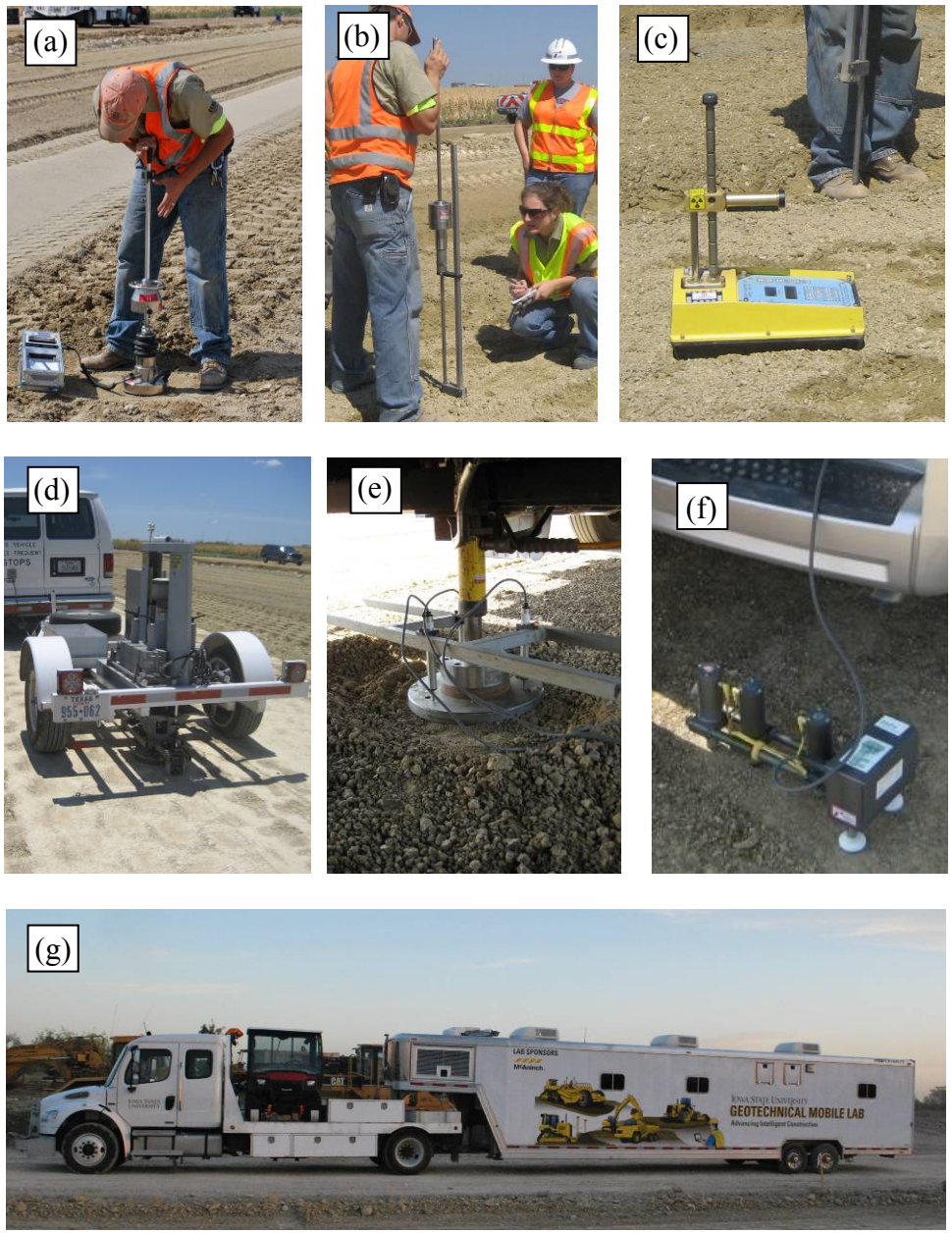

Figure 5. In-situ testing methods used on the project: (a) 200-mm diameter plate Zorn LWD, (b) dynamic cone penetrometer, (c) calibrated nuclear moisture-density gauge, (d) 300-mm diameter Dynatest FWD, (e) 300-mm diameter static PLT, (f) D-SPA, and (g) Iowa State University geotechnical mobile lab

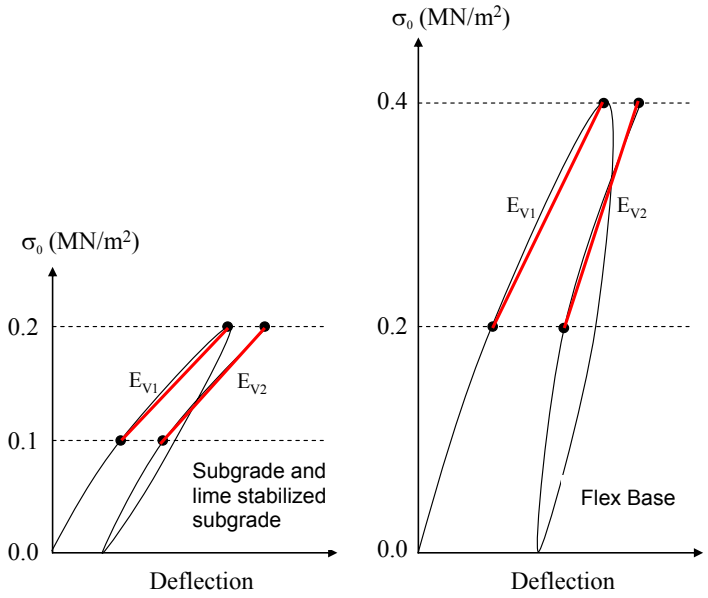

Figure 6. E_{V1} and E_{V2} determination procedure from static PLT for subgrade and flex base material

IN-SITU TEST RESULTS AND DISCUSSION

Results and analysis from this field investigation are presented in the following sections. First, brief description of the construction process, and results showing comparison between roller MVs and in-situ point measurements, spatial maps, regression analysis, and conclusions are presented separately for each testbed. Later, comparison measurements obtained between smooth drum and padfoot roller measurements from TBs 1, 3, 4, and 5 are presented. In the end, a general summary and conclusions from this field investigation and recommendations for future work are provided.

TBs 1 and 3 – Clay Subgrade Material

Construction of TBs

TB 1 was constructed by scarifying the existing subgrade material to a depth of about 250 mm. The TB was compacted in five lanes where two lanes were used as calibration test strips and the rest was used for production compaction (see Figure 7 and Figure 8). Lane 1 was prepared with three target moisture sections with moisture contents varying from dry to wet of the materials' optimum moisture content as shown on Figure 7. Lane 2 was prepared with a target moisture content close to the optimum moisture content (Figure 7). The Case/Ammann pad foot roller was used for compacting the test bed. In-situ point measurements (w, γ_d, CBR, and $E_{LWD\text{-}Z2}$) were obtained after 1, 2, 4, and 8 roller passes in the calibration lanes. Following calibration testing, the test bed was mapped using the padfoot roller. The same area was mapped using the Case/Ammann smooth drum roller (results are identified as TB 3). A few select point locations along Lanes 1 and 5 of TB 3 were also tested to determine $E_{FWD\text{-}D3}$, E_{V1}, w, γ_d, and CBR values, following mapping passes.

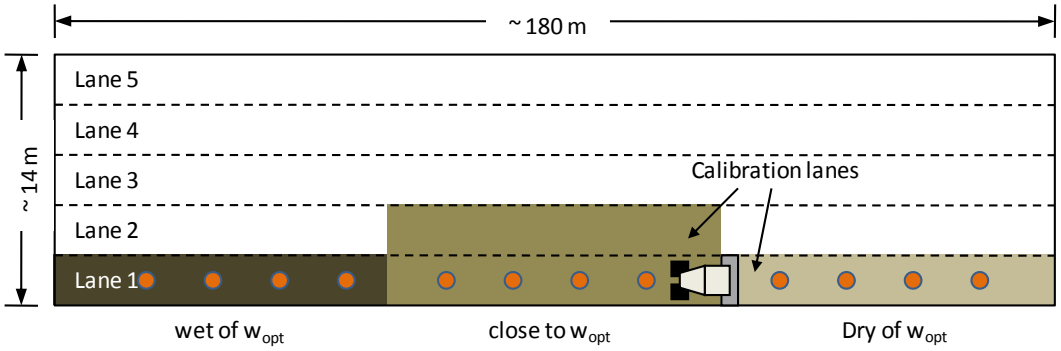

Figure 7. Experimental testing setup TB 1

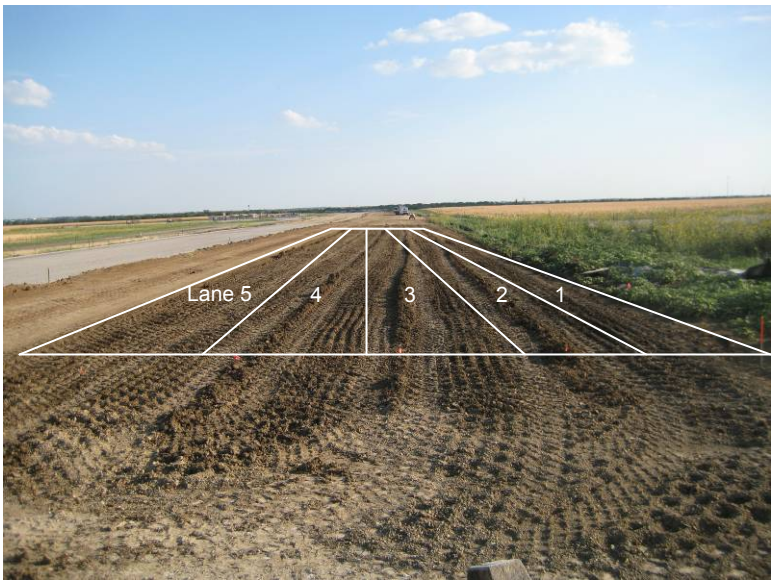

Figure 8. Picture showing different lanes on TB 1

Roller-integrated and in-situ point measurements

Roller-integrated k_{sIPD} results for various passes from calibration lane 1 are provided in Figure 9 which indicates that the results are repeatable. Multiple pass k_{sIPD} maps of TB 1 are presented in Figure 10. The maps indicate increasing compaction based on k_{sIPD} measurement values increasing with increasing passes. Figure 11 shows the average k_{sIPD} and in-situ measurement compaction growth curves for each moisture section. A reduction in k_{sIPD} was noticed after pass 1 and then a consistent increase in compaction was noticed from pass 2 to 8. This behavior is likely due to the first pass knocking down the rough ground condition. The dry of optimum moisture content and optimum moisture sections showed comparatively better growth in k_{sIPD} and in-situ point measurement values compared to the wet section. No significant increase was noticed in the average γ_d values from pass 4 to 8 for the wet of optimum and optimum moisture sections. Figure 12 presents in-situ w-γ_d results after pass 8 in comparison with laboratory w-γ_d relationships determined from standard and modified Proctor tests. After

pass 8, on average the dry of optimum, close to optimum, and wet of optimum sections of the subgrade were at about 96%, 89%, and 88% of the standard Proctor γ_{dmax}.

Comparison between k_{slPD} and different in-situ point measurements for calibration lanes 1 and 2 are presented in
Figure 13. The $E_{LWD\text{-}Z2}$ point measurements captured the variability observed in the k_{slPD} measurements better than the CBR and γ_d measurements. Using the mapping pass measurements from the padfoot (TB 1) and smooth drum rollers (TB3), comparison between k_{slPD}, k_{slSD} and in-situ point measurements are presented in Figure 14 for lanes 1 and 5. Results show that $E_{FWD\text{-}D3}$ and E_{V1} measurements tracked well with k_s measurement values and the other point measurements showed significant scatter.

Simple linear regression relationships between k_s and different in-situ point measurements from TBs 1 and 3 are presented in Figure 15 and Figure 16. The relationships were developed by pairing spatially nearest point measurements with the k_s data. Spatial locations of point measurements were adjusted up to ± 0.5 m between roller passes to pair with appropriate roller measurement values and involved some judgment. A summary of regression relationships from TBs 1 and 3 are presented in Table 3. The relationships show R^2 values ranging from 0 to 0.7. Relationships with E_{FWD} and E_{V1} measurements produced comparatively higher correlations with $R^2 > 0.6$.

To further assess scatter observed in the regressions, full depth CBR profiles from TB 1 were analyzed as shown in Figure 17 and Figure 18. CBR values for the underlying subgrade layer were determined (average CBR from 250 to 500 mm depth) and compared with the k_s values. This comparison indicates that in the dry of optimum portion of calibration lane 1 (i.e., position 120 m to 180 m) where the compaction layer CBR > 13, the k_s values are better correlated with the underlying layer CBR values. In the wet of optimum portion (i.e., position 0 to 60 m) where the compaction layer CBR < 8 the k_s values are better correlated with the compaction layer CBR values. This finding suggests that the roller-integrated k_s values are influenced by "soft" zones in the compaction layer as well as below the compaction layer. The γ_d, CBR, and $E_{LWD\text{-}Z2}$ measurements represent only the compaction layer (i.e., within 250 mm depth) properties and therefore did not match well with k_s measurements which were influenced by the underlying "soft" layers. The E_{V1} and $E_{FWD\text{-}D3}$ measurements are believed to have greater influence depths due to larger plate diameter (300 mm) and higher applied contact stresses. Therefore, the E_{V1} and $E_{FWD\text{-}D3}$ produced better correlations with the k_s values. Relating full depth (up to 1m) DCP-CBR profile information to correlate with k_s values is a topic of ongoing research for the research team.

Summary

Both padfoot and smooth drum roller-integrated k_s values (k_{slPD} and k_{slSD}) reliably indicate the compaction quality of the subgrade clay material with good repeatability. Regression relationships between k_s and different in-situ point measurements show positive correlations with varying degree of uncertainty in the correlations (as assessed by the R^2 values), however. Correlations with E_{FWD} and E_{V1} values (with $R^2 > 0.6$) produced better R^2 values compared to $E_{LWD\text{-}Z2}$, γ_d, and CBR (of the compaction layer) measurements. Poorer correlations with $E_{LWD\text{-}Z2}$, γ_d, and CBR compaction layer values is attributed to the limitation of shallow measurement influence depth of these measurements (≤ 250 mm). CBR profiles up to 1 m generated from DCP tests identified "soft"

zones below the compaction layer which affected the k_s values. The E_{V1} and $E_{FWD\text{-}D3}$ are believed to have influence depths that extend below the compaction layer due to higher applied contact stresses at the surface.

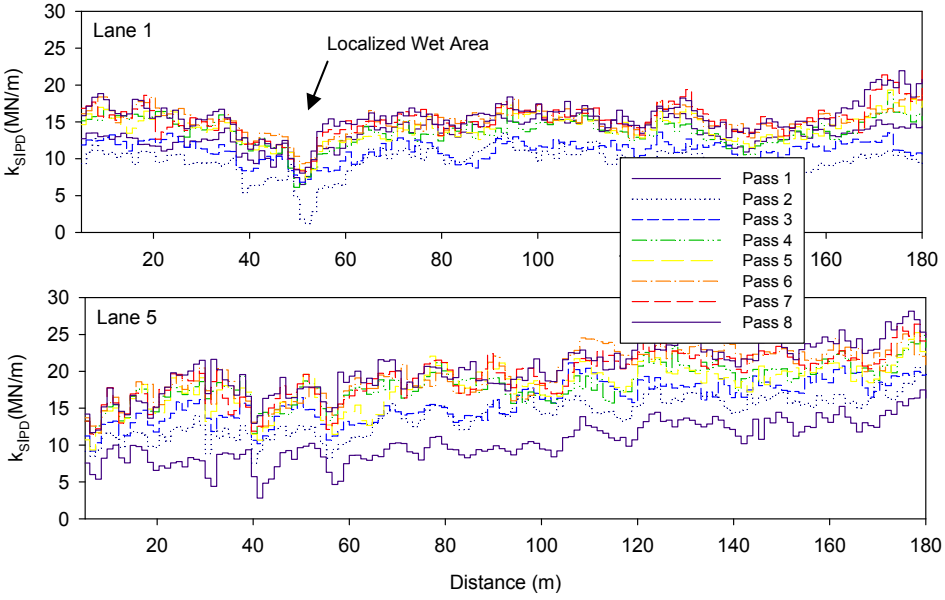

Figure 9. k_{SIPD} measurement from different passes on TB1 lanes 1 and 5 (nominal a = 0.8 mm, f = 35 Hz, and v = 3.5 km/h)

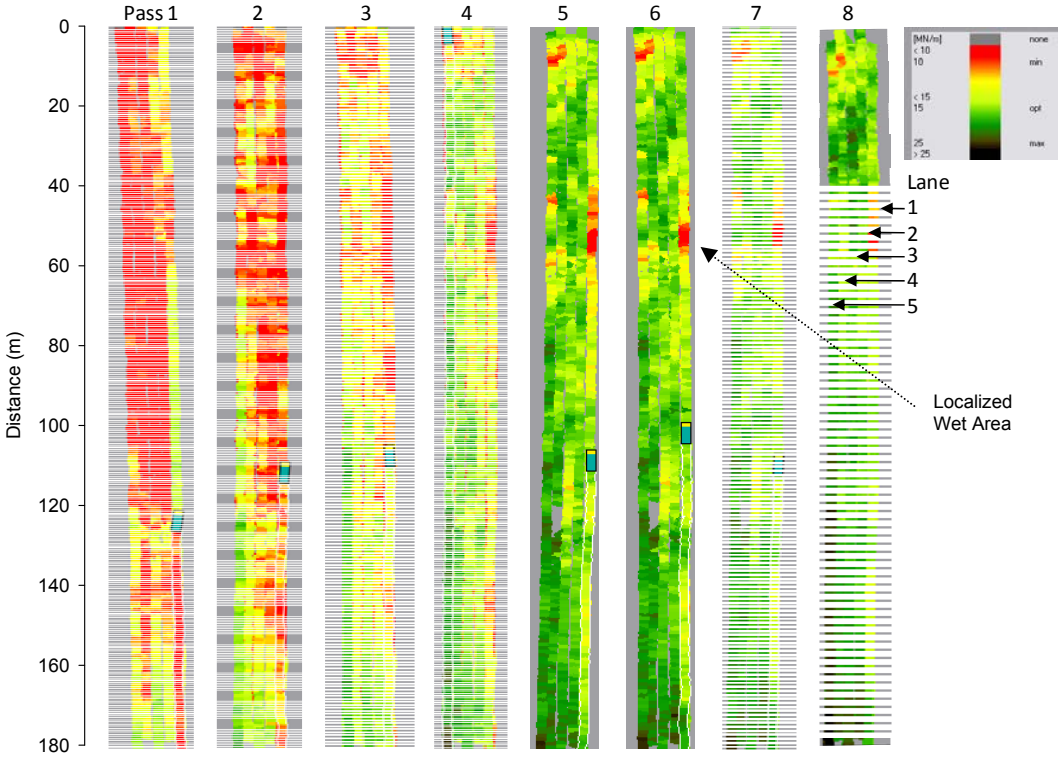

Figure 10. Screen shots of k_{SIPD} maps for different passes on TB 1

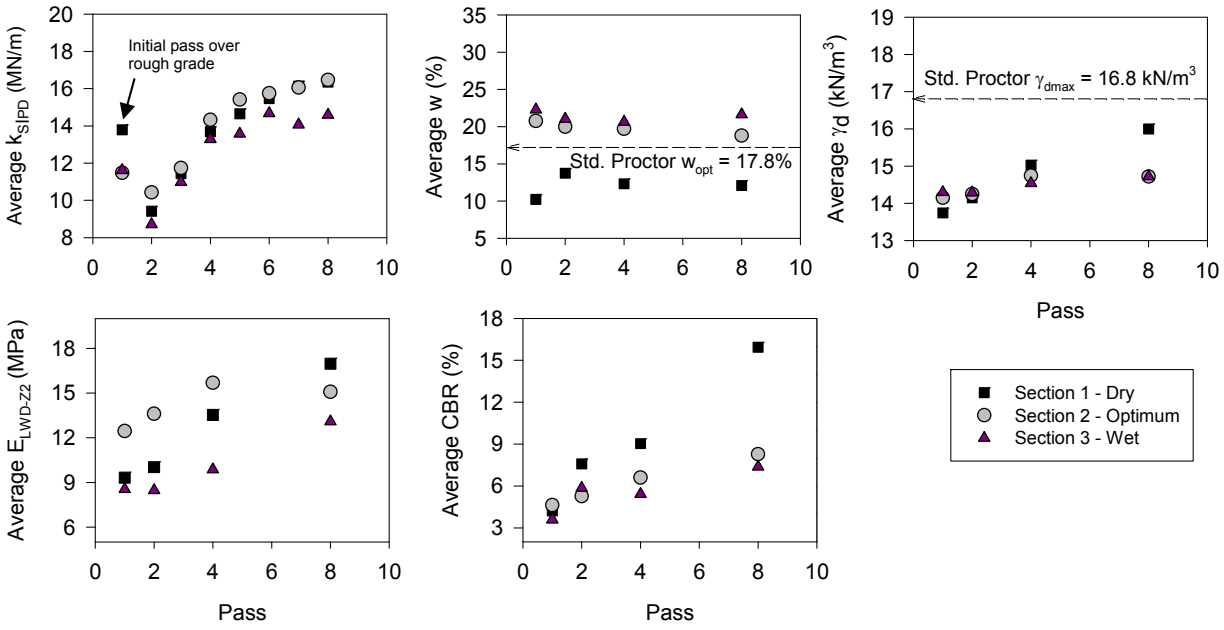

Figure 11. Compaction growth curves for k_{SIPD} and in-situ point measurements (TB 1 lane 1 calibration test strip, nominal a = 0.8 mm, f = 35 Hz, and v = 3.5 km/h)

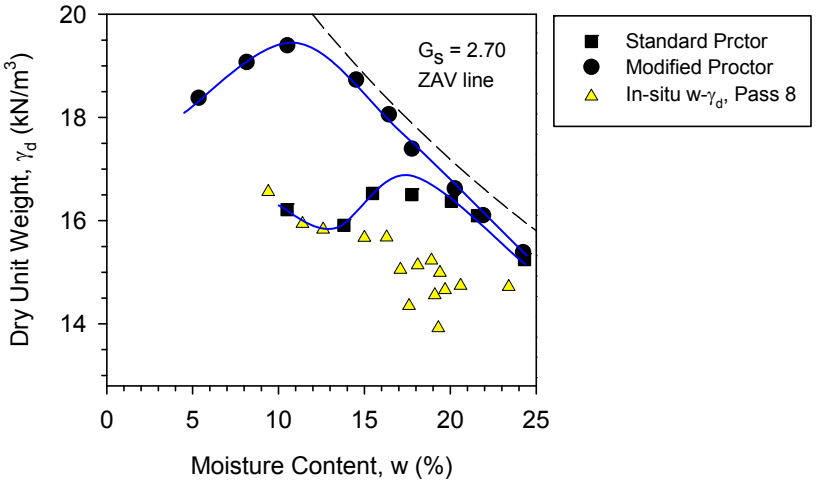

Figure 12. Comparison of laboratory Proctor curves and in-situ w-γ_d measurements after pass 8 – TB 1 subgrade material

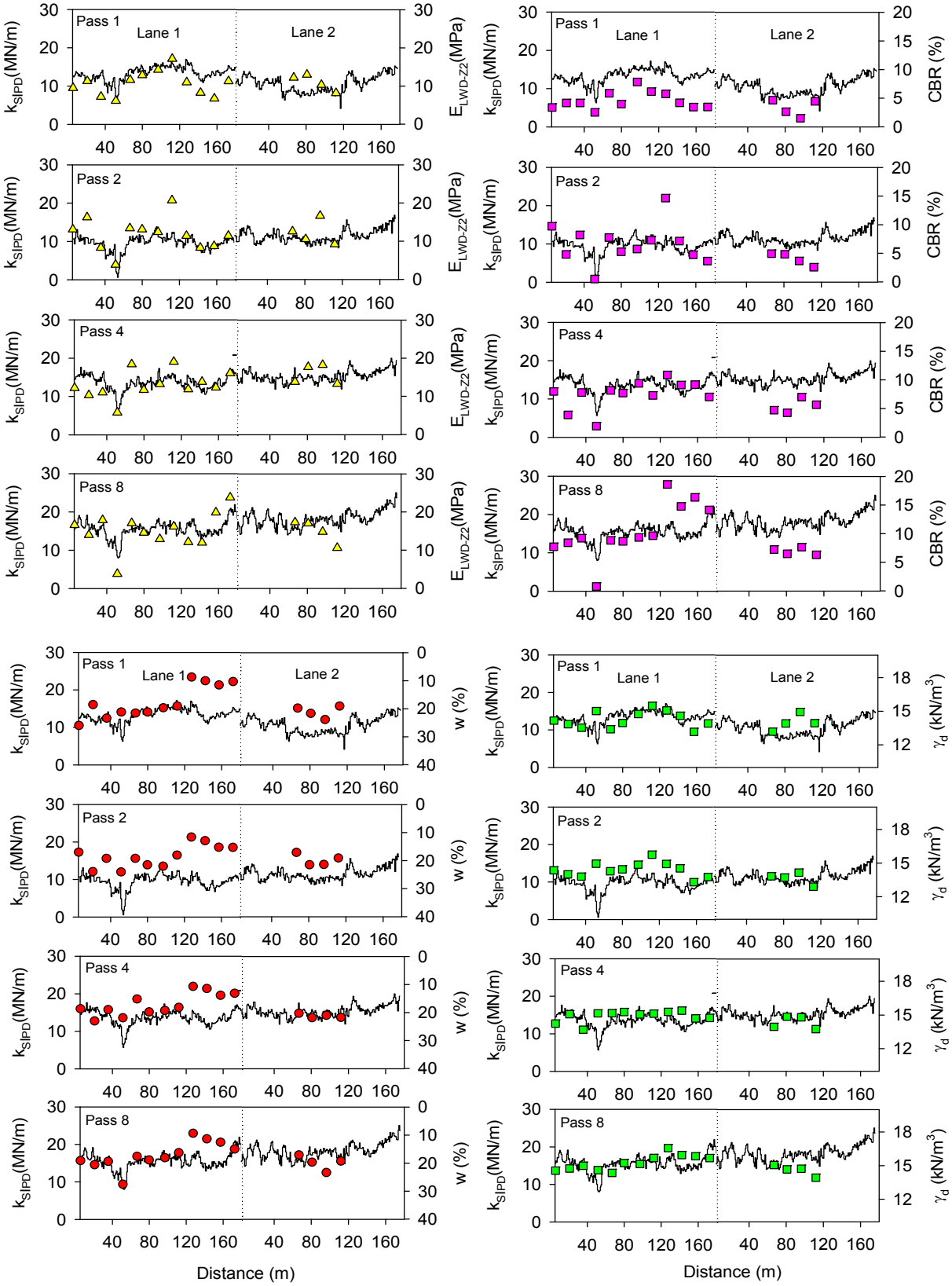

Figure 13. Comparison between k_{SIPD} and in-situ point measurements at passes 1, 2, 4, and 8 (TB 1 lane 1, nominal a = 0.8 mm, f = 35 Hz, and v = 3.5 km/h)

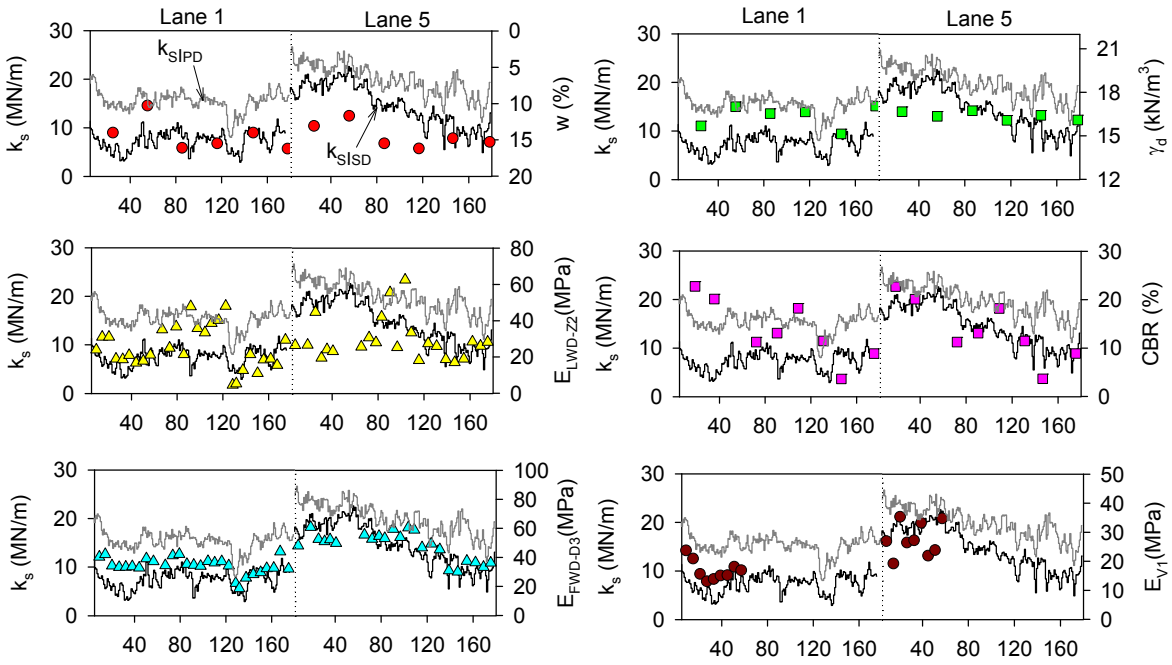

Figure 14. Comparison between k_{SIPD}, k_{SISD}, and in-situ point measurements from TB3 (k_{SISD}: mapping pass, a = 1.1 mm, f = 30 Hz, v = 3.5 km/h; k_{SIPD}: pass 8, a = 0.8 mm, f = 35 Hz, v = 3.5 km/h)

Table 3. Summary of simple linear regression analysis – TBs 1 and 3

TB	Settings	Drum	Model*	n	b_0	b_1	R^2
1/3	a = 0.8 mm f = 35 Hz	Padfoot	$k_{s\|PD} = b_0 + b_1 E_{LWD-Z2}$	120	11.60	0.17	0.29
			$k_{s\|PD} = b_0 + b_1 \gamma_d$	75	-14.50	1.92	0.33
			$k_{s\|PD} = b_0 + b_1$ CBR	81	10.69	0.43	0.40
			$k_{s\|PD} = b_0 + b_1 E_{V1}$	18	8.51	0.49	0.72
			$k_{s\|PD} = b_0 + b_1 E_{V2}$	18	11.20	0.16	0.50
			$k_{s\|PD} = b_0 + b_1 E_{FWD-D3}$	53	6.38	0.25	0.63
			$k_{s\|PD} = b_0 + b_1 E_{D-SPA}$	48	7.20	0.03	0.47
1/3	a = 1.1 mm f = 30 Hz	Smooth	$k_{s\|SD} = b_0 + b_1 E_{LWD-Z2}$	56	7.86	0.10	0.10
			$k_{s\|SD} = b_0 + b_1 \gamma_d$	12		NS†	
			$k_{s\|SD} = b_0 + b_1$ CBR	17	5.44	0.39	0.37
			$k_{s\|SD} = b_0 + b_1 E_{V1}$	18	-4.16	0.79	0.67
			$k_{s\|SD} = b_0 + b_1 E_{V2}$	18	-0.32	0.27	0.45
			$k_{s\|SD} = b_0 + b_1 E_{FWD-D3}$	53	-2.78	0.33	0.75
			$k_{s\|SD} = b_0 + b_1 E_{D-SPA}$	48	1.78	0.03	0.29

*Units: k_s (MN/m), γ_d (kN/m^3), CBR (%), E_{LWD-Z2}/E_{V1}/E_{V2}/E_{FWD-D3}/E_{D-SPA} (MPa).

† NS – not statistically significant according to $p < 0.10$ and $t < -2$ or $> +2$.

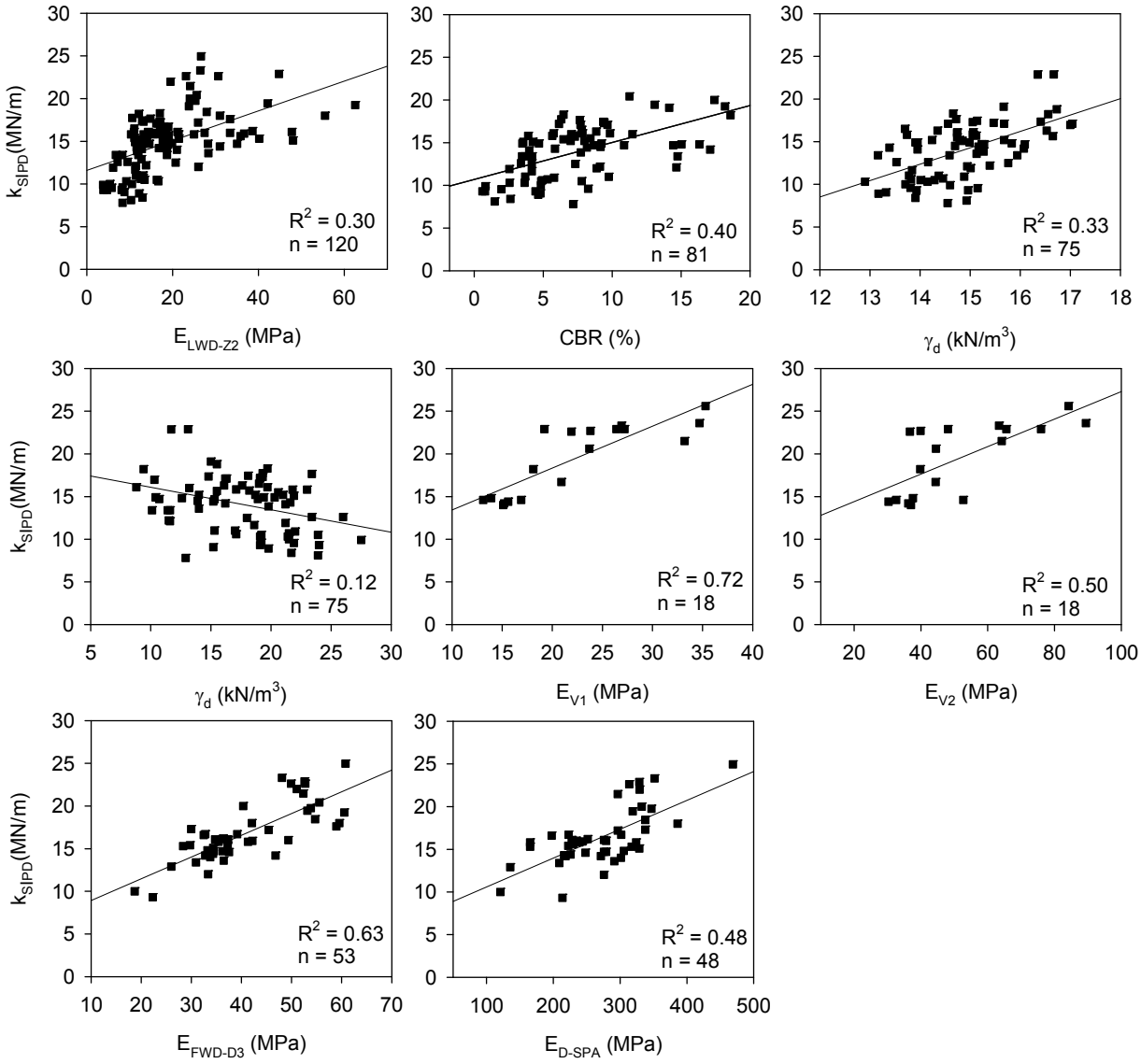

Figure 15. Simple linear regression relationships between k_{SIPD} and in-situ point measurements (TB 1 – subgrade clay material, nominal a = 0.8 mm, f = 35 Hz, and v = 3.2 km/h)

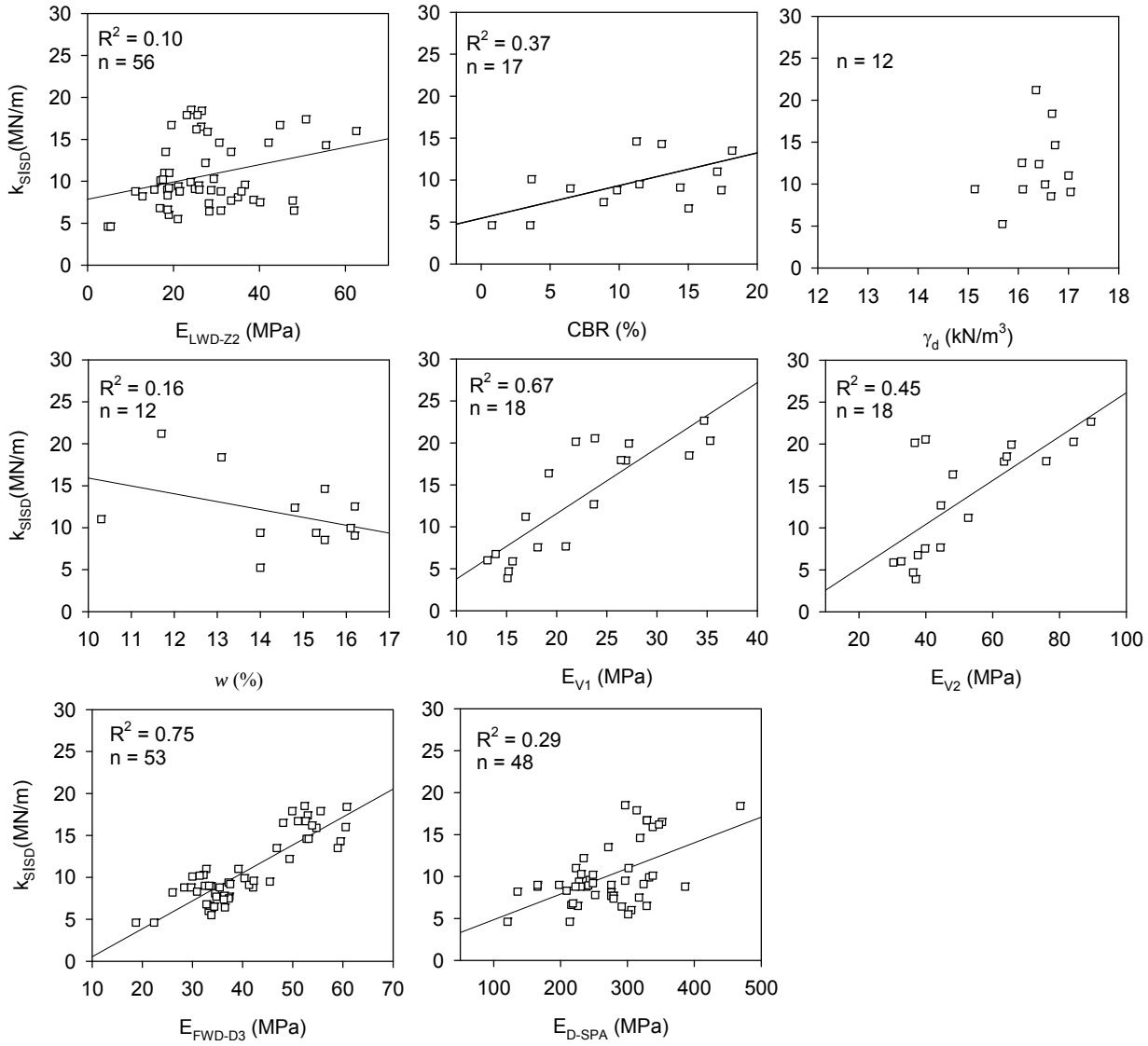

Figure 16. Simple linear regression relationships between k_{SISD} and in-situ point measurements (TB 1 – subgrade clay material, nominal a = 1.1 mm, f = 30 Hz, and v = 3.5 km/h)

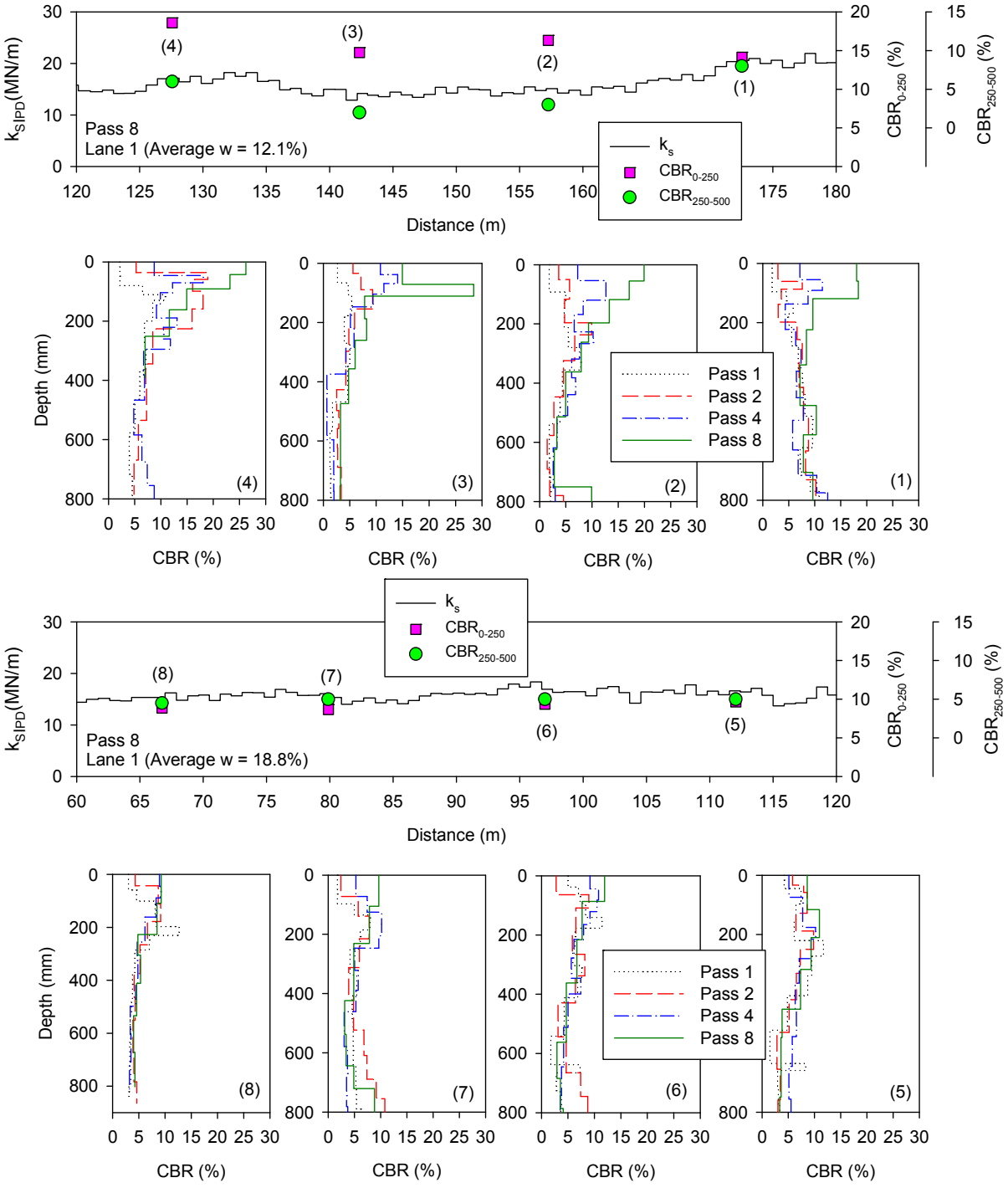

Figure 17. Comparison between roller MV and CBR profiles from TB 1 – lane 1 between 60 to 180 m (pass 8, nominal a = 0.8 mm, f = 35 Hz, and v = 3.5 km/h)

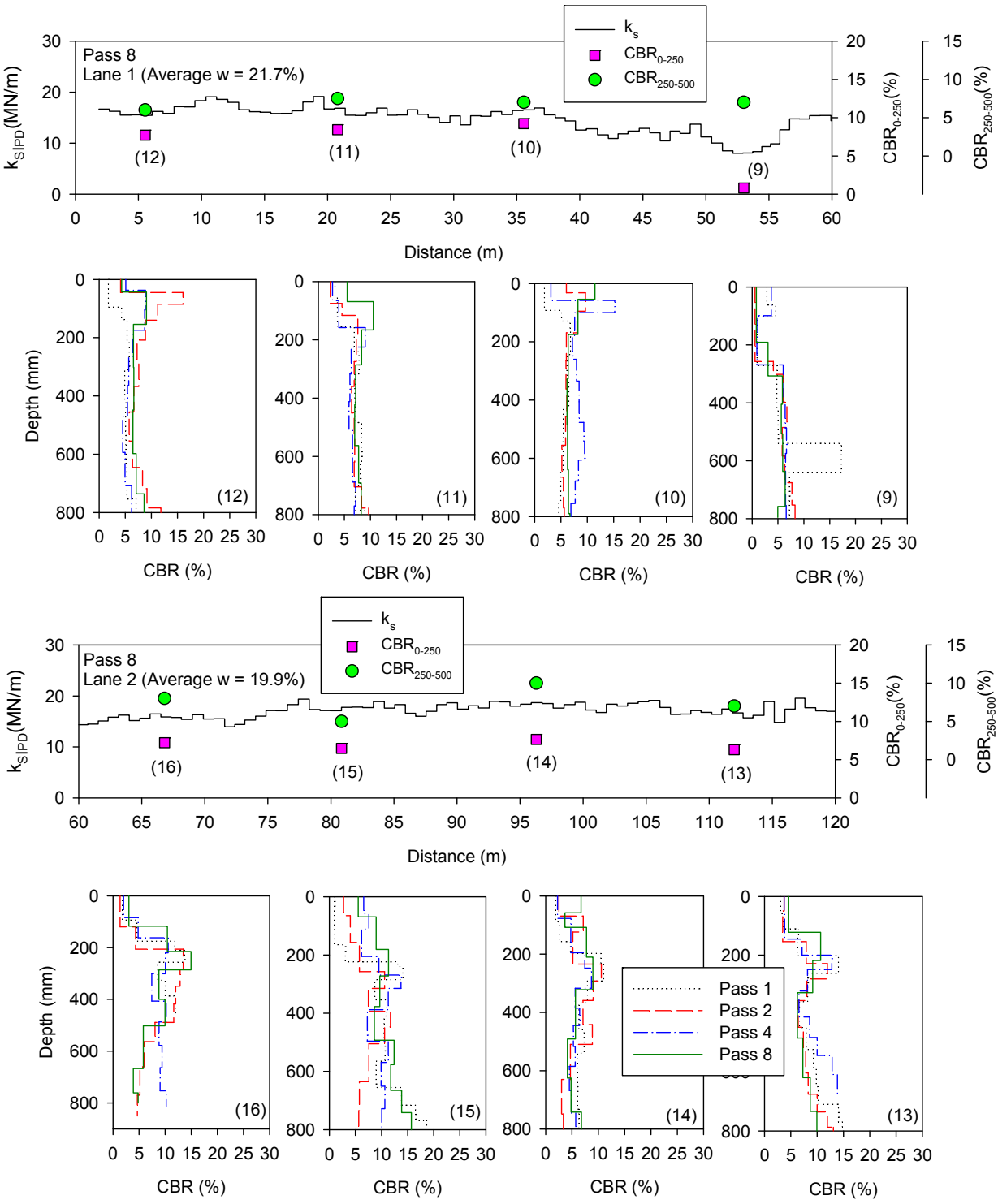

Figure 18. Comparison between roller MV and CBR profiles from TB 1 – lane 1 between 0 and 60 m, and lane 2 between 60 and 120 m (pass 8, nominal *a* = 0.8 mm, *f* = 35 Hz, *v* = and 3.5 km/h)

TB 2 lime-stabilized subgrade and flex base material

Construction and testing on TB2

TB 2 consisted of a compacted layer of lime stabilized subgrade material transitioning to flex base at each end of the TB (Figure 19). The flex base layer was significantly stiffer than the stabilized subgrade material and provided a field condition to evaluate the ability of the roller to distinguish between different ground conditions. Case/Ammann and Dynapac smooth drum rollers were used for mapping the TB with different amplitude settings (Figure 20). Following mapping passes, in-situ point measurements (w, γ_d, CBR, $E_{LWD\text{-}Z2}$, $E_{FWD\text{-}D3}$, and $E_{D\text{-}SPA}$) were obtained from lane 2 of the test bed (see Figure 20).

Roller-integrated and in-situ point measurements

Spatial maps of roller-integrated k_{SlSD} and CMV (from two different amplitude settings) are presented in Figure 20. Comparison results from lane 2 between CMV, k_{SlSD} and in-situ point measurements are presented in Figure 21 and Figure 22. Results indicate that the wide variation in stiffness of the two materials in the test bed were well-captured by the in-situ point measurements and the two roller MVs. A box culvert located at a location within the lime stabilized subgrade portion of the test bed was well captured by the roller MVs (see Figure 21 and Figure 22). CMV measurements at the two amplitude settings were similar and reproducible (see Figure 22).

Regression relationships based on spatially paired nearest point data are presented in Figure 23, and the relationships are summarized in Table 4. Results generally show separate linear trends for the lime stabilized and flex base materials. Linear regression analysis indicates comparatively better correlations with E_{FWD} measurements than with other point measurements. Hyperbolic regression relationships are provided for E_{FWD} and $E_{D\text{-}SPA}$ measurements combining measurements on flex base and lime stabilized subgrade materials. These relationships are presented only to demonstrate the trends, however, additional data is needed especially for CMV between 50 and 100, and k_s between 30 and 50 to validate the relationships.

Summary

Both roller MVs and in-situ point measurements captured the wide variation in stiffness of the compacted lime stabilized and flex base materials. A box-culvert located beneath the lime stabilized subgrade was identified with high roller MVs in that location. Linear regression relationships generally indicate separate linear trends for the lime stabilized and flex base materials. E_{FWD} measurements produced better correlations than other point measurements. Hyperbolic regression relationships were developed for E_{FWD} and $E_{D\text{-}SPA}$ measurements which showed strong correlations with k_s and CMV measurements but additional data is needed to validate the relationships. The CMV measurements at this location were highly repeatable.

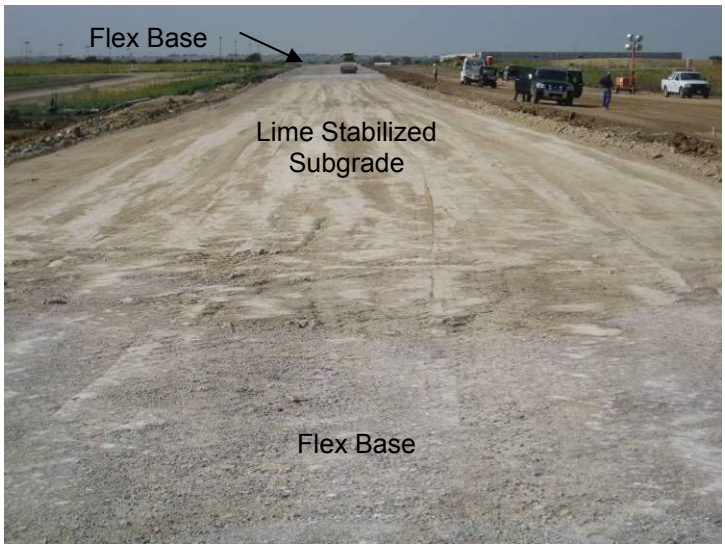

Figure 19. Picture of TB2 with flex base (on both ends of the test bed) and lime stabilized subgrade

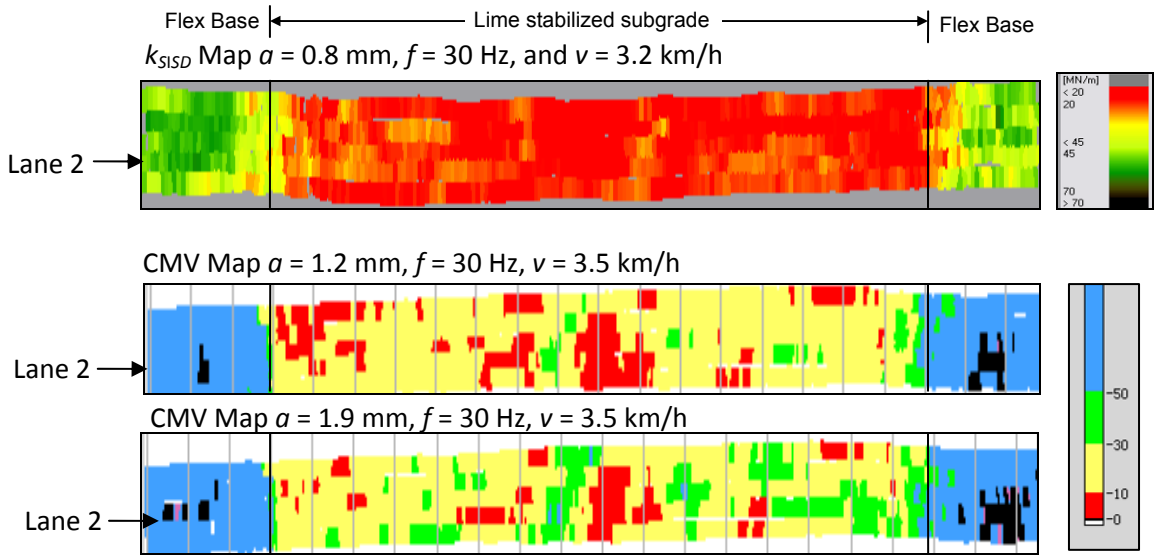

Figure 20. Comparison between k_{SISD} CMV maps– TB2 flex base and lime-stabilized subgrade

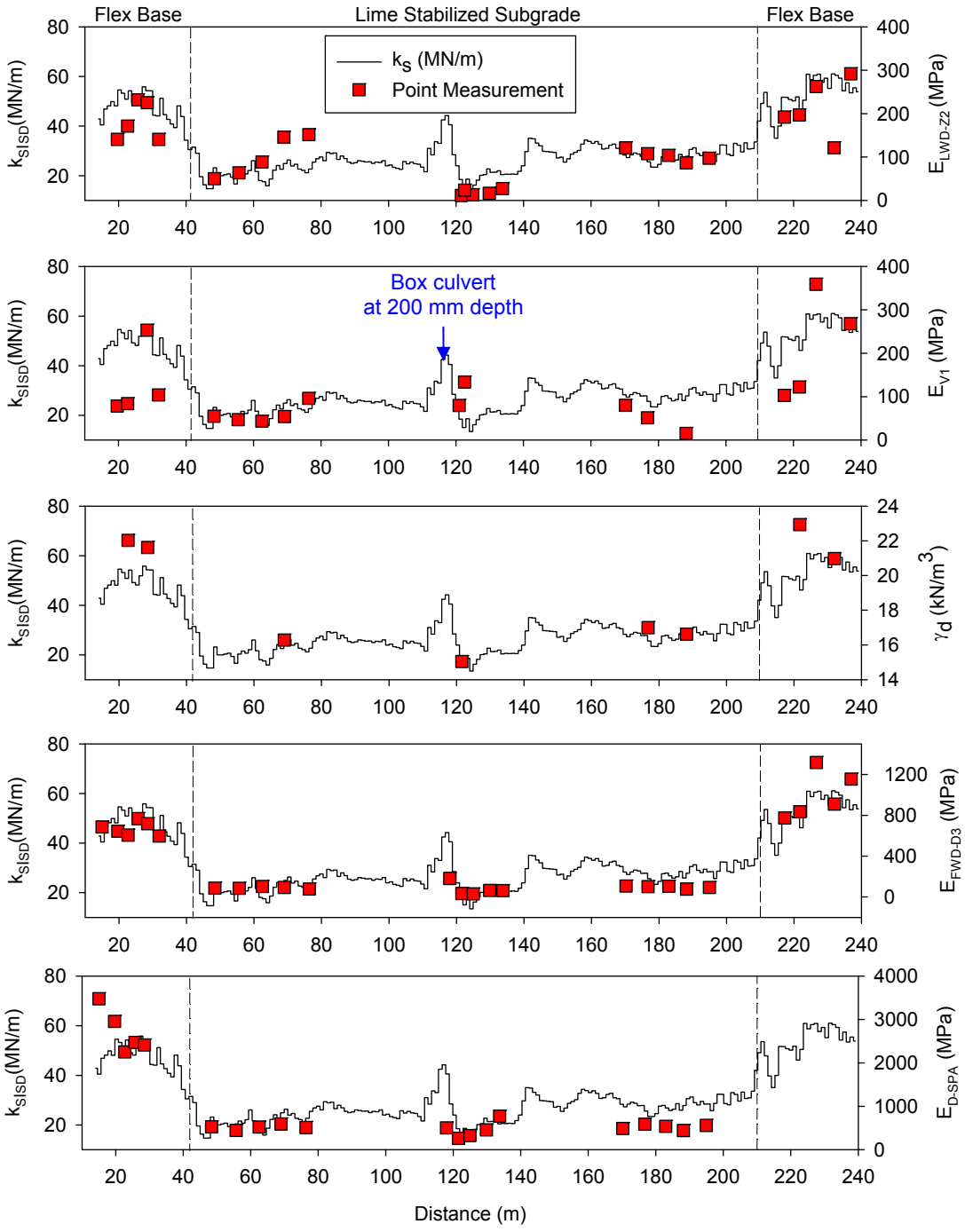

Figure 21. Comparison between k_{SISD} and in-situ point measurements – TB2 (lane 2) flex base and lime stabilized subgrade (nominal a = 0.8 mm, f = 30 Hz, and v = 3.2 km/h)

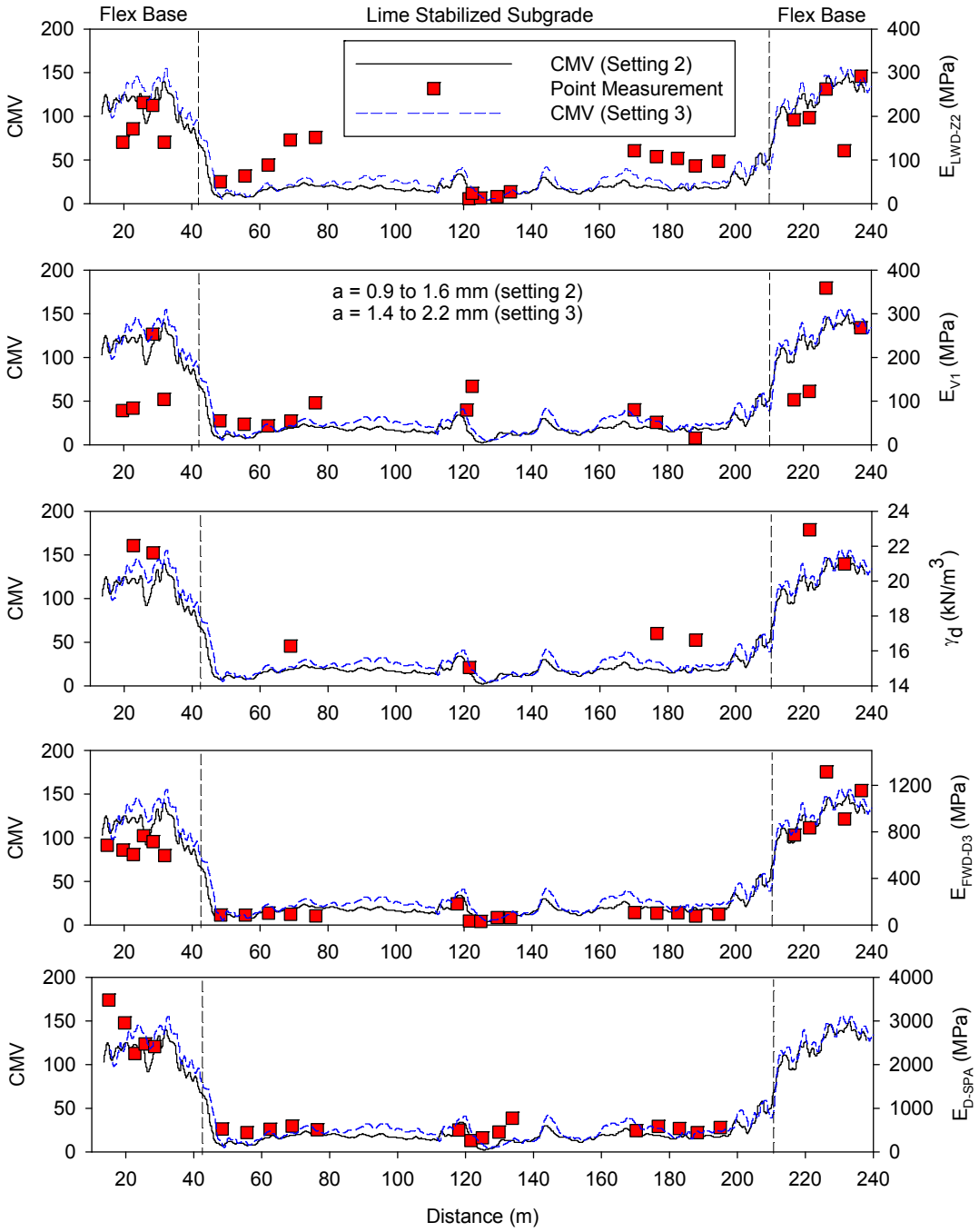

Figure 22. Comparison between CMV and in-situ point measurements – TB2 (lane 2) flex base and lime-stabilized subgrade (nominal *f* = 30 Hz and *v* = 3.2 km/h)

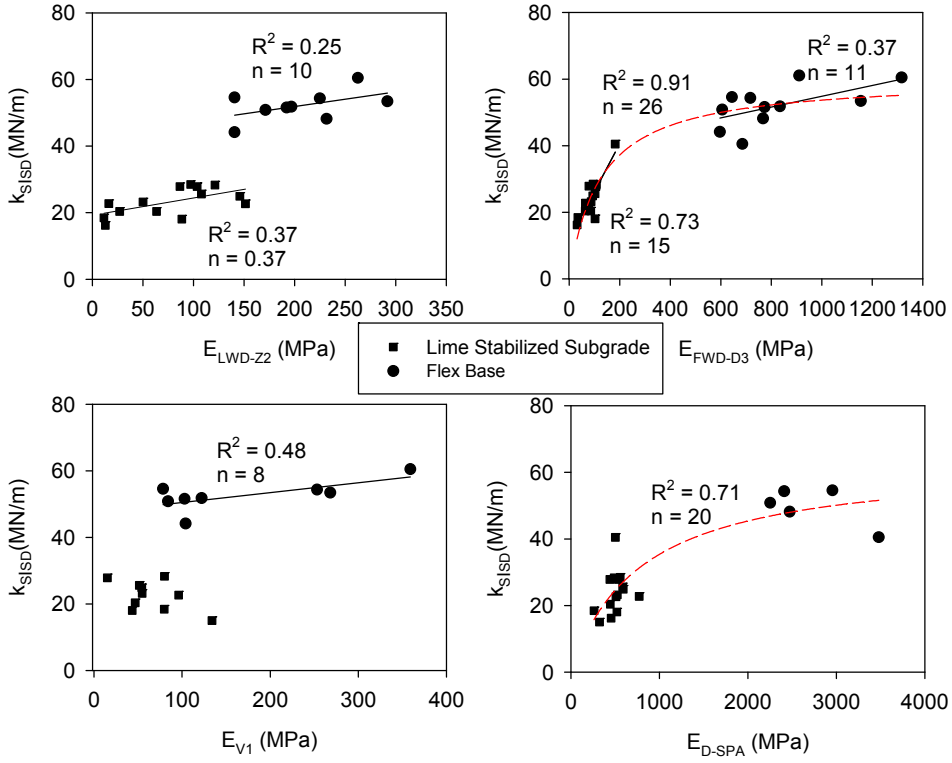

(a)

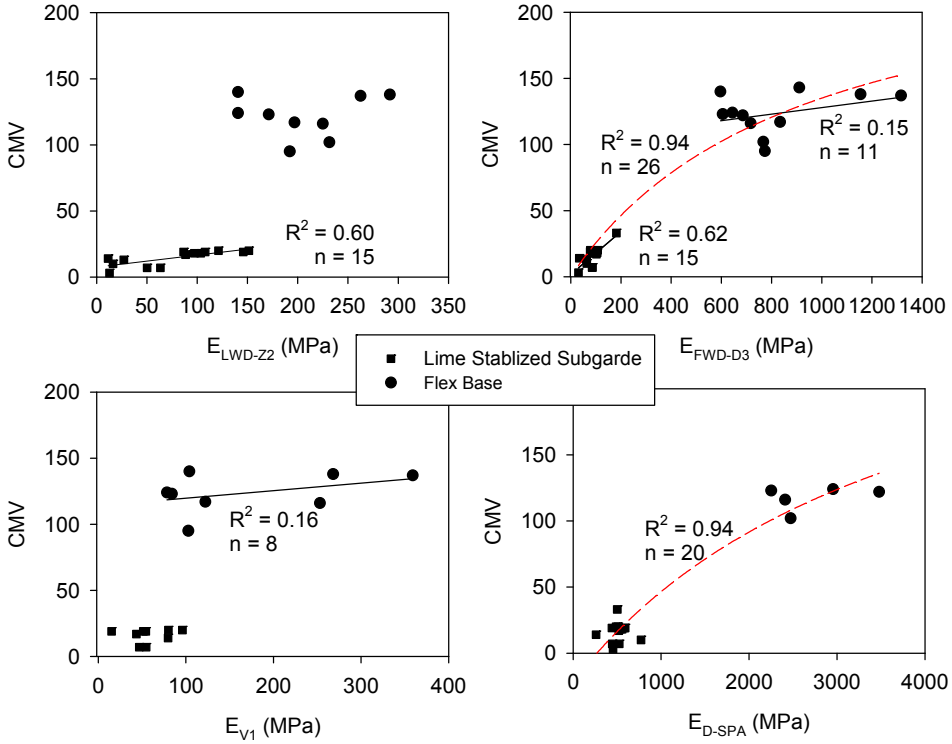

(b)

Figure 23. Simple linear regression relationships between (a) k_{SIPD}, (b) CMV and in-situ point measurements – TB 2

Table 4. Summary of simple linear regression analysis – TB 2

MV	Material*	Model**	n	b_0	b_1	R^2
$k_{s\|SD}$	LS	$k_{s\|SD} = b_0 + b_1 E_{LWD-Z2}$	15	0.05	19.18	0.37
		$k_{s\|SD} = b_0 + b_1 E_{V1}$	10		NS†	
		$k_{s\|SD} = b_0 + b_1 E_{FWD-D3}$	15	0.14	11.83	0.73
		$k_{s\|SD} = b_0 + b_1 E_{D-SPA}$	15		NS†	
	FB	$k_{s\|SD} = b_0 + b_1 E_{LWD-Z2}$	10	0.04	43.2	0.25
		$k_{s\|SD} = b_0 + b_1 E_{V1}$	8	0.03	47.5	0.48
		$k_{s\|SD} = b_0 + b_1 E_{FWD-D3}$	11	0.03	38.55	0.37
		$k_{s\|SD} = b_0 + b_1 E_{D-SPA}$	5		NS†	
	LS and FB	$k_{s\|SD} = b_0 E_{FWD-D3}/(b_1 E_{FWD-D3})$	26	60.3	124.3	0.91
		$k_{s\|SD} = b_0 E_{FWD-D3}/(b_1 E_{D-SPA})$	20	63.3	790.7	0.71
CMV	LS	$CMV = b_0 + b_1 E_{LWD-Z2}$	15	0.09	7.46	0.60
		$CMV = b_0 + b_1 E_{V1}$	10		NS†	
		$CMV = b_0 + b_1 E_{FWD-D3}$	15	0.16	1.79	0.62
		$CMV = b_0 + b_1 E_{D-SPA}$	15		NS†	
	FB	$CMV = b_0 + b_1 E_{LWD-Z2}$	10		NS†	
		$CMV = b_0 + b_1 E_{V1}$	8	0.06	114.05	0.16
		$CMV = b_0 + b_1 E_{FWD-D3}$	11	0.02	103.19	0.15
		$CMV = b_0 + b_1 E_{D-SPA}$	5		NS†	
	LS and FB	$CMV = b_0 E_{FWD-D3}/(b_1 E_{FWD-D3})$	26	259.6	921.9	0.94
		$CMV = b_0 E_{FWD-D3}/(b_1 E_{D-SPA})$	20	336.0	3930.3	0.94

*LS – lime stabilized subgrade, FB – flex base

*Units: k_s (MN/m), γ_d (kN/m^3), CBR (%), $E_{LWD-Z2}/E_{V1}/E_{V2}/E_{FWD-D3}/E_{D-SPA}$ (MPa).

† NS – not statistically significant according to $p < 0.10$ and $t < -2$ or $> +2$.

TB 5 lime-stabilized subgrade material

Construction of TB

TB 5 consisted of lime-treated subgrade material and was located in the same area as TB 2. Prior to mapping operations on TB 2, on 07/21/2008 the existing subgrade material was scarified to a depth of about 250 mm, reclaimed with lime slurry, and compacted using padfoot and smooth drum rollers (Figure 24). The application of lime slurry was observed to be non-uniform across the test bed (Figure 25) because of ponding in the center of the test bed. The compacted layer was reclaimed using a soil pulverizer and moisture conditioned on 07/23/2008 to prepare TB5 (Figure 24). Compaction operations on TB 5 were performed by dividing the area into six roller lanes (see Figure 27 and Figure 28). Three lanes were compacted using Case/Ammann padfoot roller and the other three lanes were compacted using Case/Ammann smooth drum roller. Lanes 3 and 4 were used as calibration test strips for padfoot and smooth drum rollers, respectively, and the remaining area was used for production compaction. In-situ point measurements (w, γ_d, CBR, and E_{LWD-Z2}) were obtained on the calibration lanes after 1, 2, 4, 8 and 12 compaction passes. The test bed was mapped using the smooth drum roller

following production compaction. E_{FWD}, $E_{D\text{-}SPA}$, E_{V1}, E_{V2}, and E_{LWD} tests were conducted on lane 1 after mapping.

To assess the influence of time delay on the compaction characteristics of the lime stabilized material, laboratory Proctor density tests were carried out at three different times (see Figure 29). As a result of increasing flocculation and agglomeration, the laboratory w-γ_d relationships indicate that the optimum moisture content increases and the maximum dry unit weight decreases with time.

Figure 24. Photos showing placement (left) and reclamation (right) process of lime slurry with existing subgrade material (pictures taken 07/21/08)

Figure 25. Picture showing ponding of lime slurry on the scarified subgrade (picture taken 07/21/2008)

Figure 26. Picture showing soil reclaiming (left) and moisture conditioning process on TB 5 (picture taken 07/23/2008)

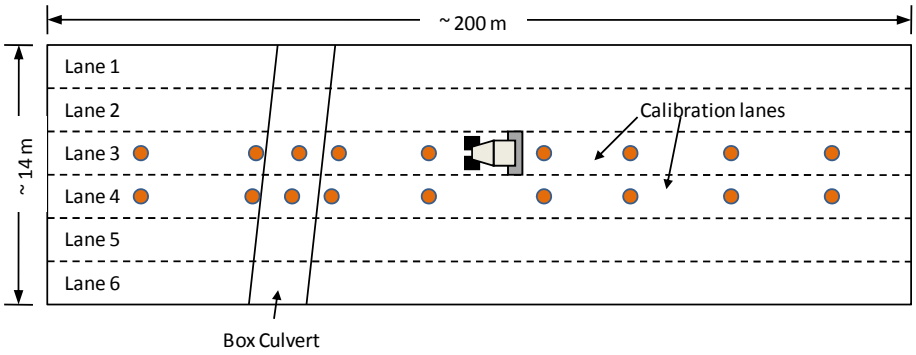

Figure 27. Experimental testing setup on TB5 (lane 3 for padfoot roller calibration strip and lane 4 for smooth drum roller calibration strip)

Figure 28. Picture of TB5 with different lanes

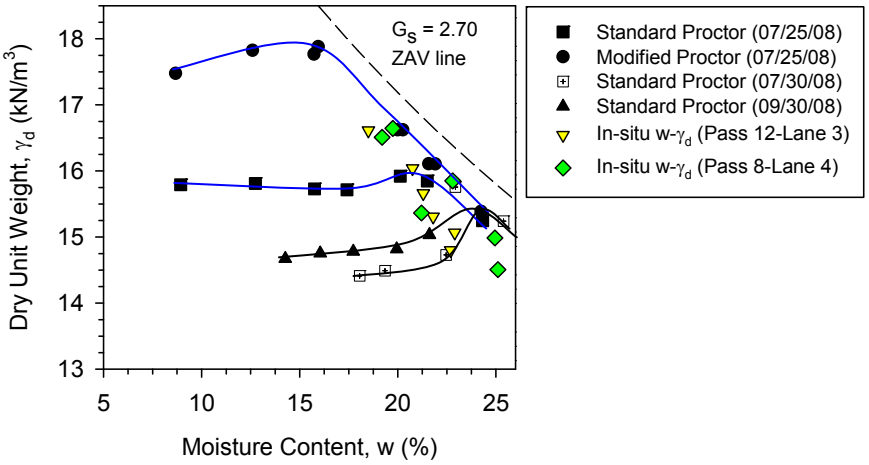

Figure 29. Comparison of laboratory Proctor curves and in-situ *w*-γ_d measurements – TB 5 lime-stabilized subgrade material

Roller-integrated and in-situ point measurements

Roller-integrated k_{sIPD} results for various passes from calibration lane 3 are provided in Figure 30 which indicates that the results are repeatable and that the values increase with increasing passes. Figure 31 shows the average k_{sIPD} and in-situ measurement compaction growth curves for the lane 3 calibration strip. The in-situ test measurements (γ_d, CBR, and E_{LWD}) reached an asymptotic maximum at 8 passes. E_{LWD} showed a reduction in the average value after 12 passes, likely because of surficial decompaction. The average k_{sIPD} value reached an asymptotic value by 8 passes and showed a slight increase from pass 11 to 12. Figure 32 shows the average in-situ measurement compaction growth curves for the lane 4 calibration strip compacted using smooth drum roller. k_{sISD} results were not available for the lane 4 calibration strip due to a corrupt data file problem.

The in-situ measurement values on average showed slightly greater compaction on lane 4 compared to lane 3 after pass 8 (γ_d = 15.0 kN/m^3 on lane 3 and 15.3 kN/m^3 on lane 4; E_{LWD} = 35 MPa on lane 3 and 39 MPa on lane 4). In-situ *w*-γ_d results after 12 and 8 passes on lanes 3 and 4, respectively, are presented in comparison with laboratory *w*-γ_d relationships in Figure 29. Results show that the material was close to or wet of optimum moisture content as determined by standard Proctor test on a sample tested on 07/25/08 (note that the soil was compacted in the field on 07/23/2008, for future testing involving stabilized subgrade it would be worthwhile to perform the lab compaction test at the same time the material is being compacted to eliminate differences in maximum dry unit weight and optimum moisture content from time dependent chemical reactions).

Comparisons between k_{sIPD} and different in-situ point measurements for calibration lane 3 and production lane 1 are presented in Figure 33 and Figure 34, respectively. The $E_{LWD\text{-}Z2}$, E_{V1}, E_{V2}, $E_{FWD\text{-}D3}$, $E_{D\text{-}SPA}$, and CBR point measurements captured the variability observed in k_{sIPD} measurements better than the γ_d measurements. The *w* measurements tracked well along the k_{sIPD}

measurements indicating that an increase in *w* causes a decrease in k_{slPD}. Using the mapping pass measurements from the smooth drum roller, k_{slSD} measurements are also presented in comparison with the in-situ point measurements in Figure 33 and Figure 34. Discussion on comparison between k_{slSD} and k_{slPD} measurements is presented later in the report.

Figure 35 shows the k_{slSD} map with CBR profiles at four select locations highlighting the area underlain by box culvert. The k_{slSD} values at the location underlain by the box culvert (about 200 mm below grade) were higher and the k_{slSD} values were lower along the edge of the culvert, which is a common condition whereby it is difficult to compact material directly adjacent to box culvert walls. CBR profiles shown in Figure 35 confirm the poor backfill compaction condition.

Simple linear regression relationships between k_s values and different in-situ point measurements from are presented in Figure 36 and Figure 37. The relationships were developed by pairing spatially nearest point measurements with the k_s data. Spatial locations of point measurements were slightly ($< \pm 0.5$ m) adjusted to pair with appropriate roller measurement value using judgment. A summary of the regression relationships are presented in Table 5. The relationships show low R^2 values for relationships with γ_d ($R^2 = 0.21$ to 0.37). Relationships with $E_{D\text{-}SPA}$ for this dataset also show poor correlations, however with encouraging trends and warrants application in future studies. Other in-situ point measurements showed good correlations with $R^2 > 0.5$. The k_s values were sensitive to moisture content as evidenced by $R^2 > 0.5$ in the regression relationships.

Summary

Both padfoot and smooth drum roller-integrated k_s values (k_{slPD} and k_{slSD}) reliably indicated the compaction quality of the lime stabilized subgrade clay material with good repeatability. The k_s measurements effectively identified poor backfill compaction conditions along the edge of a box culvert located in this test bed and the results were confirmed from CBR profiles. Regression relationships between k_s and different in-situ point measurements show positive correlations with varying degree of uncertainty in the correlations (as assessed by the R^2 values), however. Better correlations were observed with E_{FWD}, E_{V1}, E_{V2}, and E_{LWD} values (with $R^2 > 0.5$) compared to $E_{D\text{-}SPA}$ and γ_d. Relationships with $E_{D\text{-}SPA}$ show encouraging trends in the data, however. The k_s values were sensitive to moisture content of the compaction layer material.

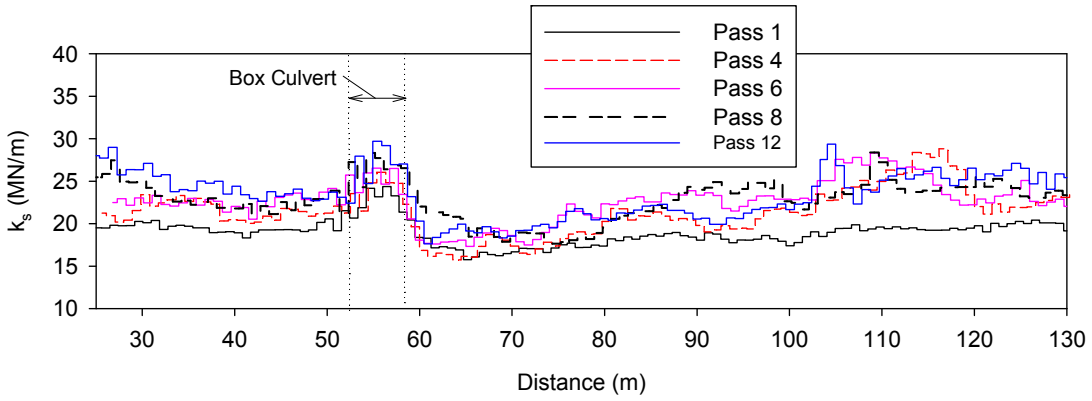

Figure 30. k_{SIPD} measurements from different passes on TB5 lane 3 calibration test strip (nominal a = 1.0 mm, f = 35 Hz, and v = 3.5 km/h)

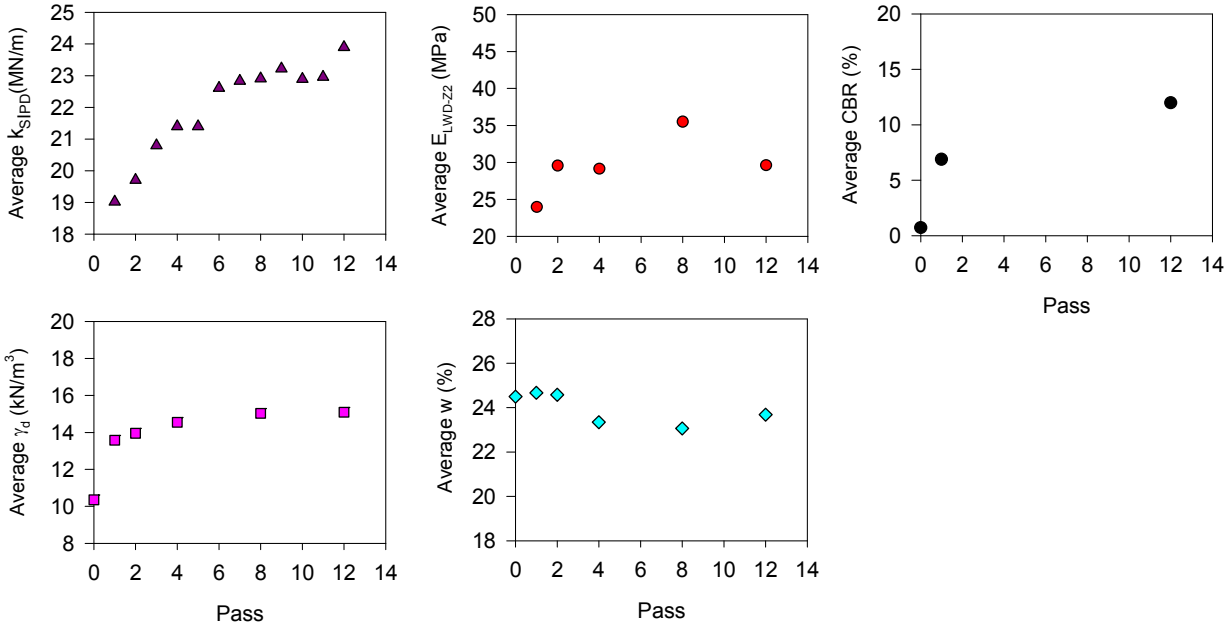

Figure 31. Compaction growth curves for k_{SIPD} and in-situ point measurements (TB 5 lane 3 calibration test strip, nominal a = 1.0 mm, f = 35 Hz, and v = 3.5 km/h)

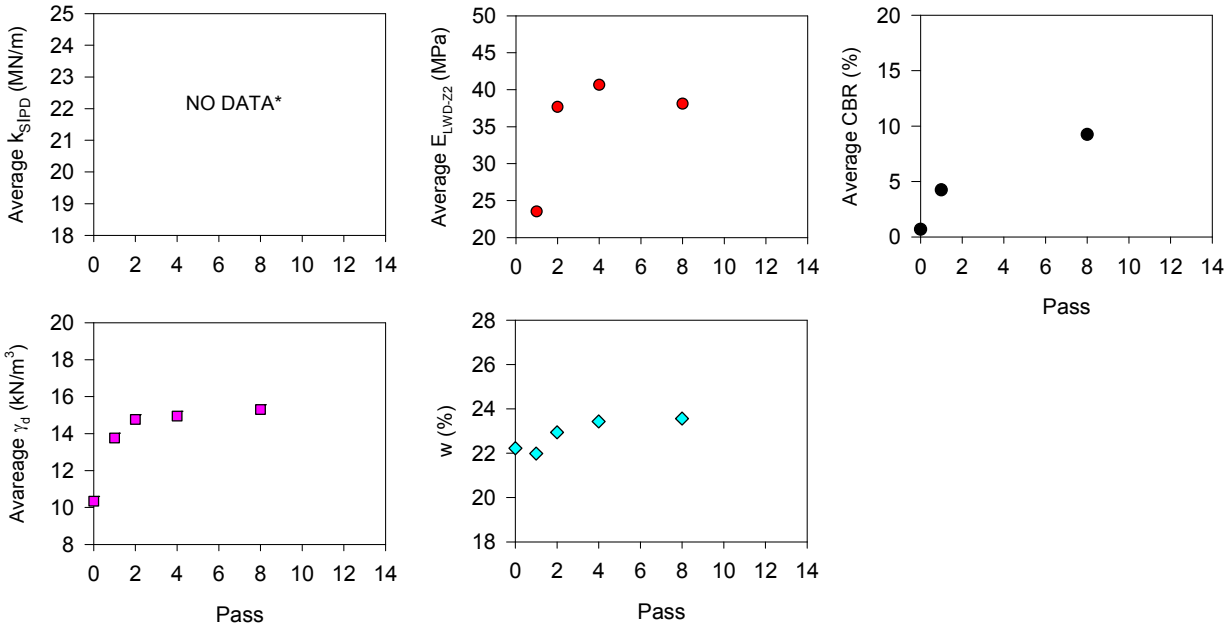

Figure 32. Compaction growth curves for in-situ point measurements (TB 5 lane 4 calibration test strip) (*roller data file corrupt)

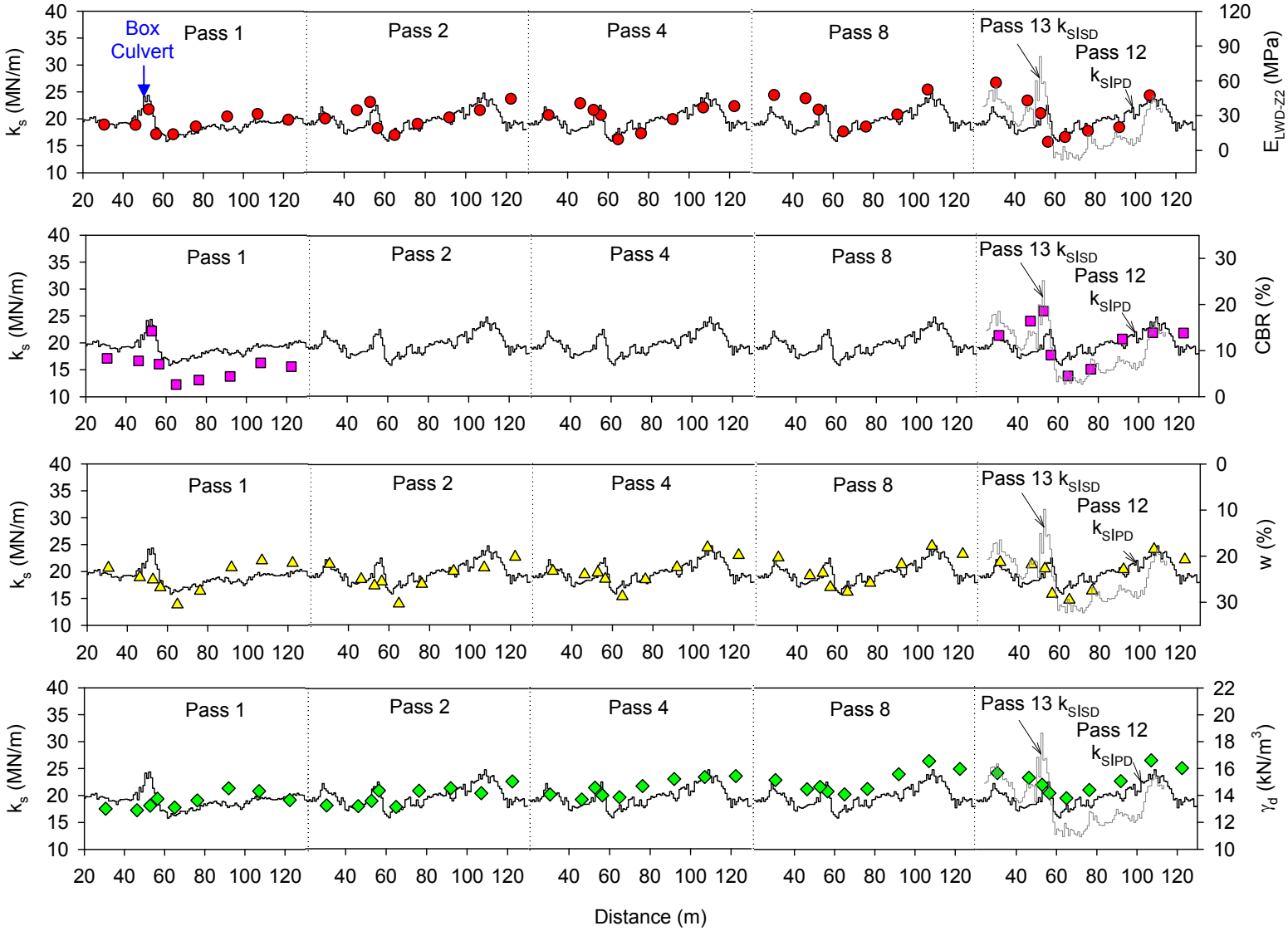

Figure 33. Comparison results between k_{SIPD} (passes 1 to 12), k_{SISD} (pass 13), and in-situ point measurements – TB5 lime stabilized subgrade calibration lane (nominal a = 1.0 mm, f = 35 Hz, and v = 3.5 km/h)

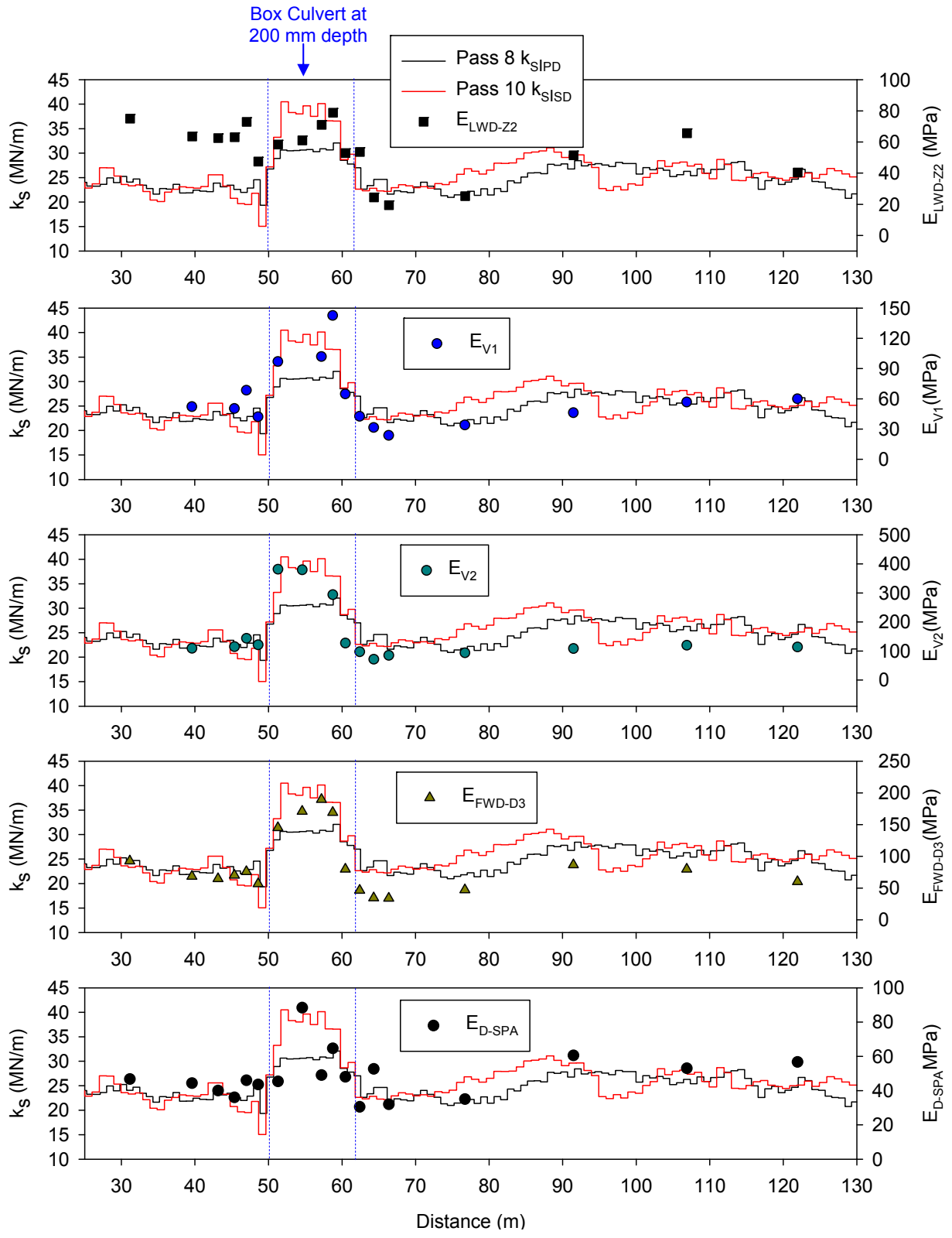

Figure 34. Comparison between k_{SIPD}, k_{SISD}, and in-situ point measurements on TB 5 – lane 1 lime stabilized subgrade material (k_{SIPD}: nominal a = 1.0 mm, f = 35 Hz, and v = 3.5 km/h; k_{SISD}: nominal a = 1.5 mm, f = 35 Hz, and v = 3.2 km/h)

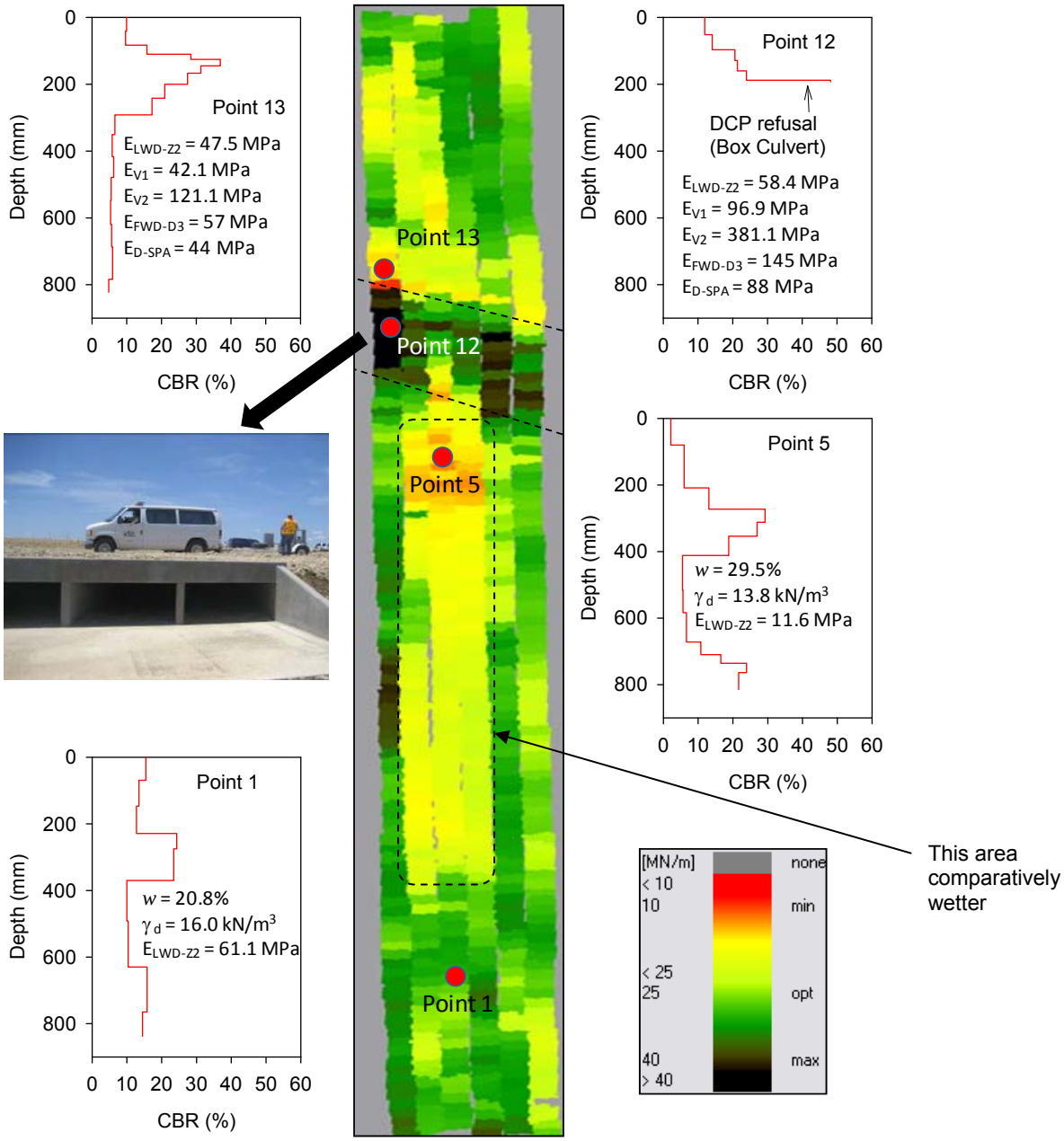

Figure 35. k_{SISD} maps (map 1: nominal a = 1.5 mm, f = 30 Hz, and v = 3.2 km/h) and DCP profiles at select locations on TB5 lime stabilized material (isolated area underlain by a concrete box culvert)

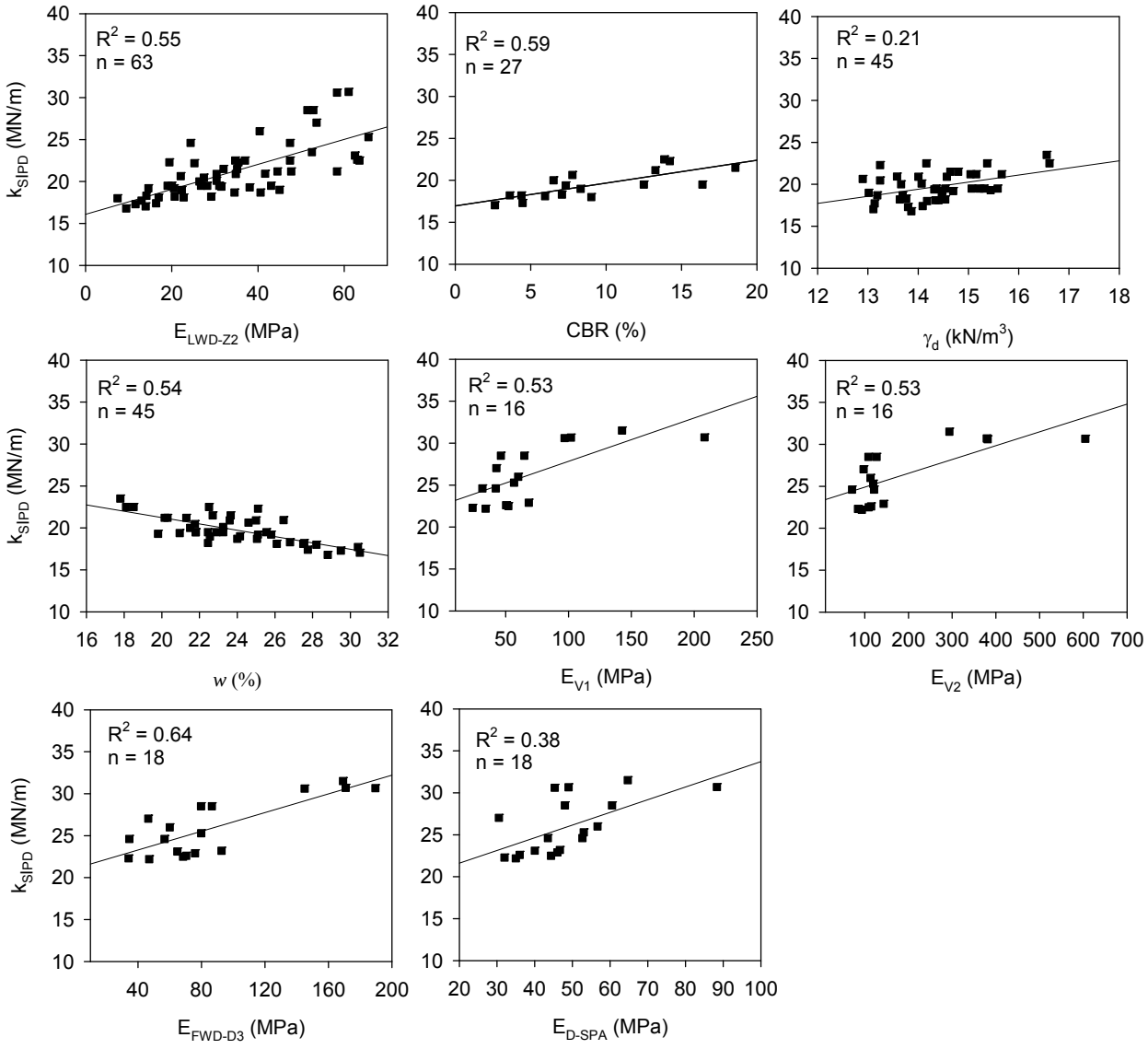

Figure 36. Simple linear regression relationships between k_{SIPD} and in-situ point measurements (TB 5 – lime stabilized subgrade clay material, nominal a = 1.0 mm, f = 35 Hz, and v = 3.2 km/h)

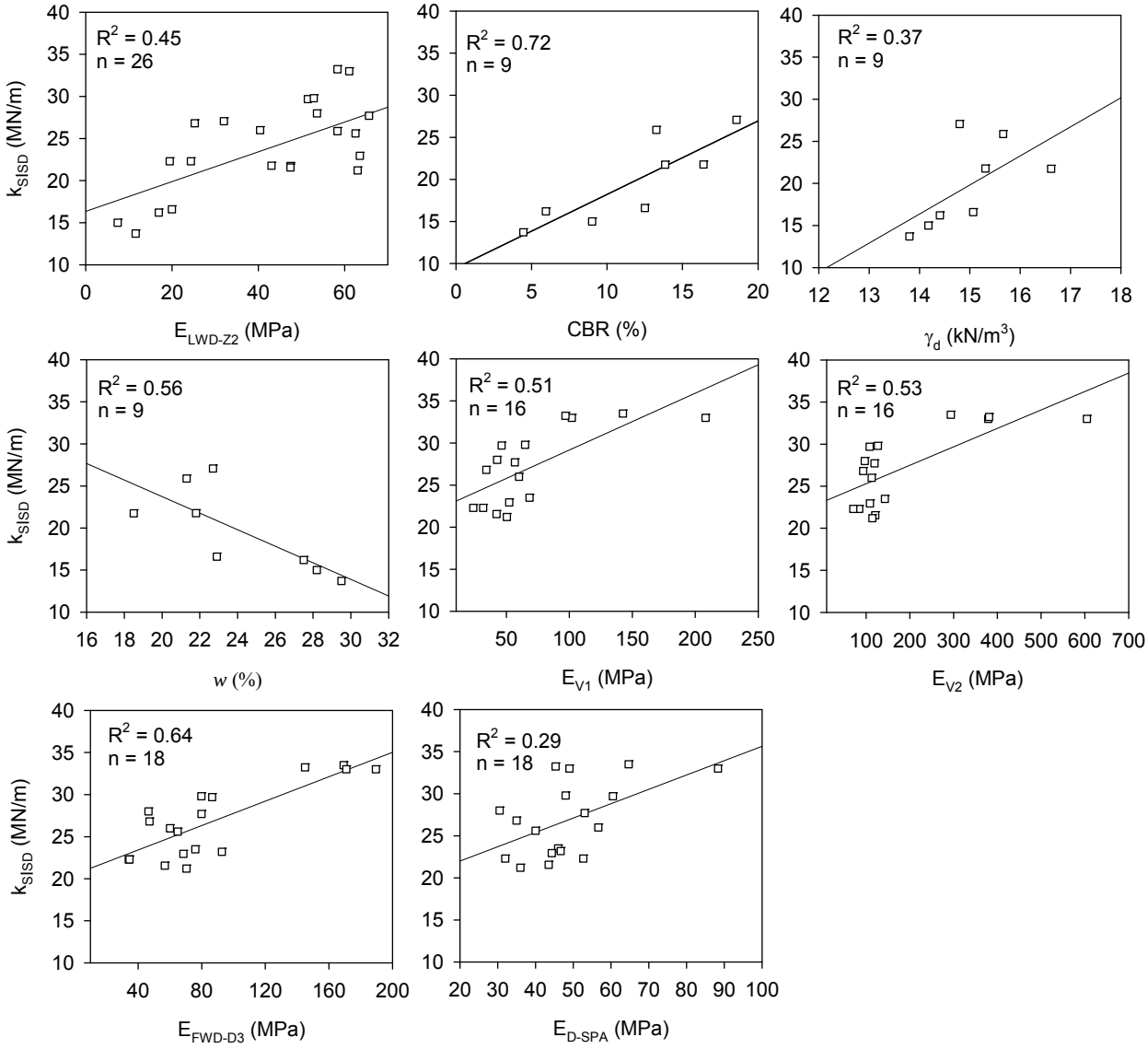

Figure 37. Simple linear regression relationships between k_{SISD} and in-situ point measurements (TB 5 – lime stabilized subgrade clay material, nominal a = 1.5 mm, f = 30 Hz, and v = 3.2 km/h)

Table 5. Summary of simple linear regression analysis – TB 5

TB	Settings	Drum	Model*	n	b_0	b_1	R^2
5	a = 0.9 mm f = 35 Hz	Padfoot	$k_{s\|PD} = b_0 + b_1 E_{LWD-Z2}$	63	16.10	0.15	0.55
			$k_{s\|PD} = b_0 + b_1 \gamma_d$	45	7.58	0.85	0.21
			$k_{s\|PD} = b_0 + b_1$ CBR	27	16.96	0.27	0.59
			$k_{s\|PD} = b_0 + b_1 E_{V1}$	16	22.66	0.05	0.53
			$k_{s\|PD} = b_0 + b_1 E_{V2}$	16	23.23	0.02	0.53
			$k_{s\|PD} = b_0 + b_1 E_{FWD-D3}$	18	21.06	0.06	0.64
			$k_{s\|PD} = b_0 + b_1 E_{D-SPA}$	18	18.60	0.15	0.38
5	a = 1.5 mm f = 30 Hz	Smooth	$k_{s\|SD} = b_0 + b_1 E_{LWD-Z2}$	26	16.35	0.18	0.45
			$k_{s\|SD} = b_0 + b_1 \gamma_d$	9	-31.96	3.45	0.37
			$k_{s\|SD} = b_0 + b_1$ CBR	9	9.48	0.87	0.72
			$k_{s\|SD} = b_0 + b_1 E_{V1}$	16	22.43	0.07	0.51
			$k_{s\|SD} = b_0 + b_1 E_{V2}$	16	23.11	0.02	0.53
			$k_{s\|SD} = b_0 + b_1 E_{FWD-D3}$	18	20.51	0.07	0.64
			$k_{s\|SD} = b_0 + b_1 E_{D-SPA}$	18	18.60	0.17	0.29

*Units: k_s (MN/m), γ_d (kN/m^3), CBR (%), $E_{LWD-Z2}/E_{V1}/E_{V2}/E_{FWD-D3}/E_{D-SPA}$ (MPa).

† NS – not statistically significant according to $p < 0.10$ and $t < -2$ or $> +2$.

TBs 6 and 7 flex base material

Construction and material conditions

TB6 consisted of approximately 150 mm to 200 mm thick flex base material placed and leveled to the project grade. Water was added on the layer using water trucks and compacted using Dynapac smooth drum roller in five roller lanes using different operation settings (see Figure 38). Lanes 1, 2, and 5 were compacted in manual mode, and lanes 3 and 4 were compacted using AFC mode. Field observations during compaction indicated water ponding at the surface due to relatively low permeability of the material (Figure 39). In contrast to the flex base layer on TB2 (which was compacted several days prior), the material was relatively soft and "spongy" during compaction passes. Compaction passes were performed on TB 6 on 07/23/2008. On 07/24/2008, the test bed was mapped using different amplitude settings (identified as TB 7). In-situ point measurements (w, γ_d, CBR, E_{LWD-Z2}, E_{FWD-D3}, E_{V1}, E_{V2}, and E_{D-SPA}) were obtained over the compacted flex base layer TB 7, following mapping operations. The E_{FWD} measurements were obtained from 180 test locations for spatial analysis. Figure 39 and Figure 40 shows pictures of TB7 after mapping. Significant moisture segregation was noticed on the compacted surface particularly across the roller drum width in a compaction lane (see Figure 40).

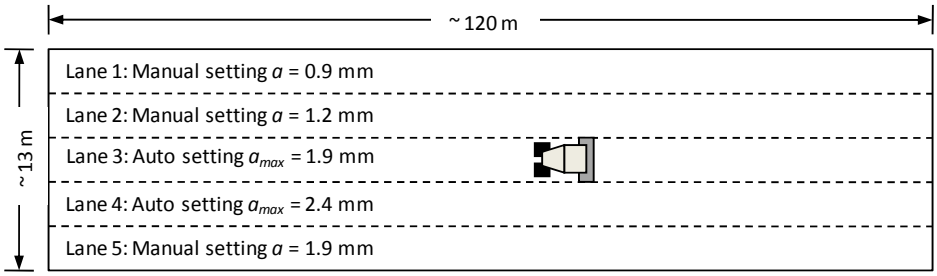

Figure 38. Experimental setup on TB 6

Figure 39. Moisture on flex base material during compaction (TB 6 left) and a day after compaction (TB 7 right)

Figure 40. Moisture segregation on flex base material during testing (TB 7)

Roller-integrated and in-situ point measurements

Roller-integrated measurement values CMV and BV for various passes on lanes 1 through 5 are provided in Figure 41 through Figure 45, respectively. No bouncing was noticed (as assed by BV measurements) for lanes 1, 2, and 4 manual mode and lane 3 AFC mode compaction.

Lane 4 which was compacted in AFC mode with a_{max} = 2.4 mm showed roller jumping within a 10 m zone as indicated on Figure 44. For this case the AFC mode did not necessarily prevent roller jumping or reduce the vibration amplitude. The CMV and BV measurement values on all lanes were repeatable.

The average CMV compaction growth curves for all lanes are presented in Figure 46. Results show no significant change in compaction with each pass on any of the lanes. On average, the CMV measurements were greater for lanes compacted with higher amplitudes. The CMV measurements obtained from this TB were in the range of 20 and 70. The CMV measurements on TB2 flex base material were greater than about 100. This indicates that the material gains significant strength over time as the material dries and is further compacted under construction traffic.

Figure 47 presents CMV maps for TB 7 from three different settings (two in manual mode and one in AFC mode). Comparison between CMV from two manual mode settings and different in-situ point measurements are presented in Figure 48, Figure 49, and Figure 50. Comparison between CMV measurements from manual setting and amplitude measurements from AFC setting are presented in Figure 51. Results indicate that the CMV measurements are influenced by amplitude, i.e., increasing amplitude increases the CMV measurement value. AFC setting with a_{max} = 2.4 mm did not produce bouncing and the amplitude value remained relatively constant at about 2.4 mm in all roller lanes. A comparison between CMV and E_{FWD} measurements showed that the point measurements tracked well with the variability in CMV for lanes 2, 4, and 5, but did not track well on lanes 1 and 3. The CMV measurements correlated well with variations with moisture content within 4% to 6% by showing a decrease in CMV with an increase in moisture content. $E_{D\text{-}SPA}$, E_{V1}, and CBR tracked well with the variations in CMV measurements on lanes 1 and 3. The reason for poor correlation with E_{FWD} measurements on lanes 1 and 3 is attributed to possible effects of heterogeneity observed in the material across the drum width due to moisture segregation. Only one point measurement was obtained at the center of the drum while the roller value is an integrated response over the full drum width. Due to this uncertainty, regression relationships are not developed for this test bed. Future testing should consider multiple measurements over the drum width for conditions where this type of heterogeneity exists.

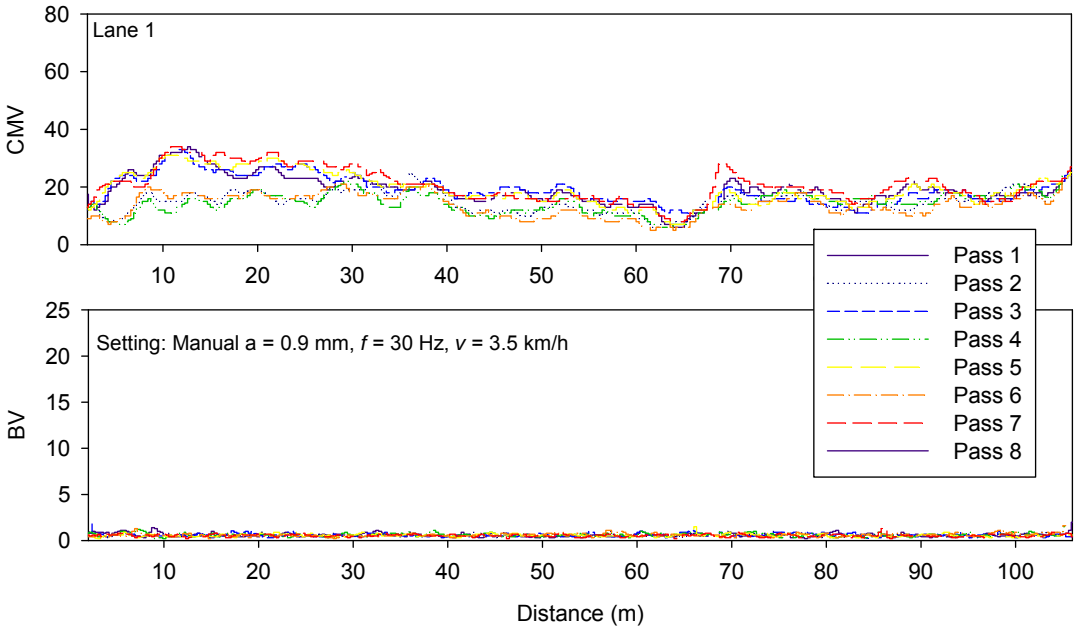

Figure 41. CMV and BV values for compaction passes on lane 1 of TB6 flex base material

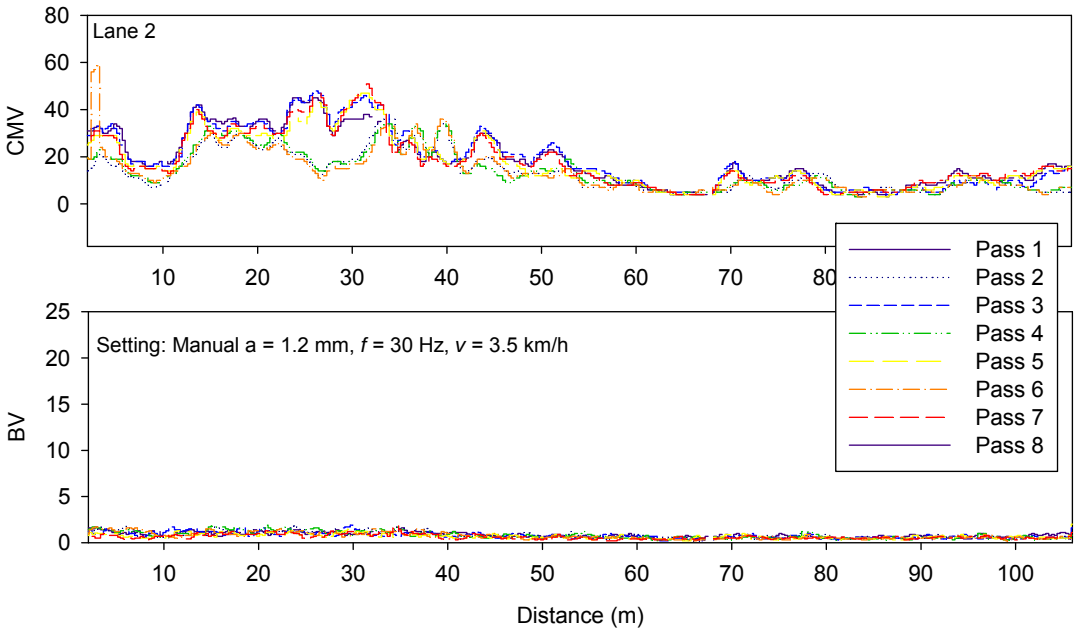

Figure 42. CMV and BV values for compaction passes on lane 2 of TB6 flex base material

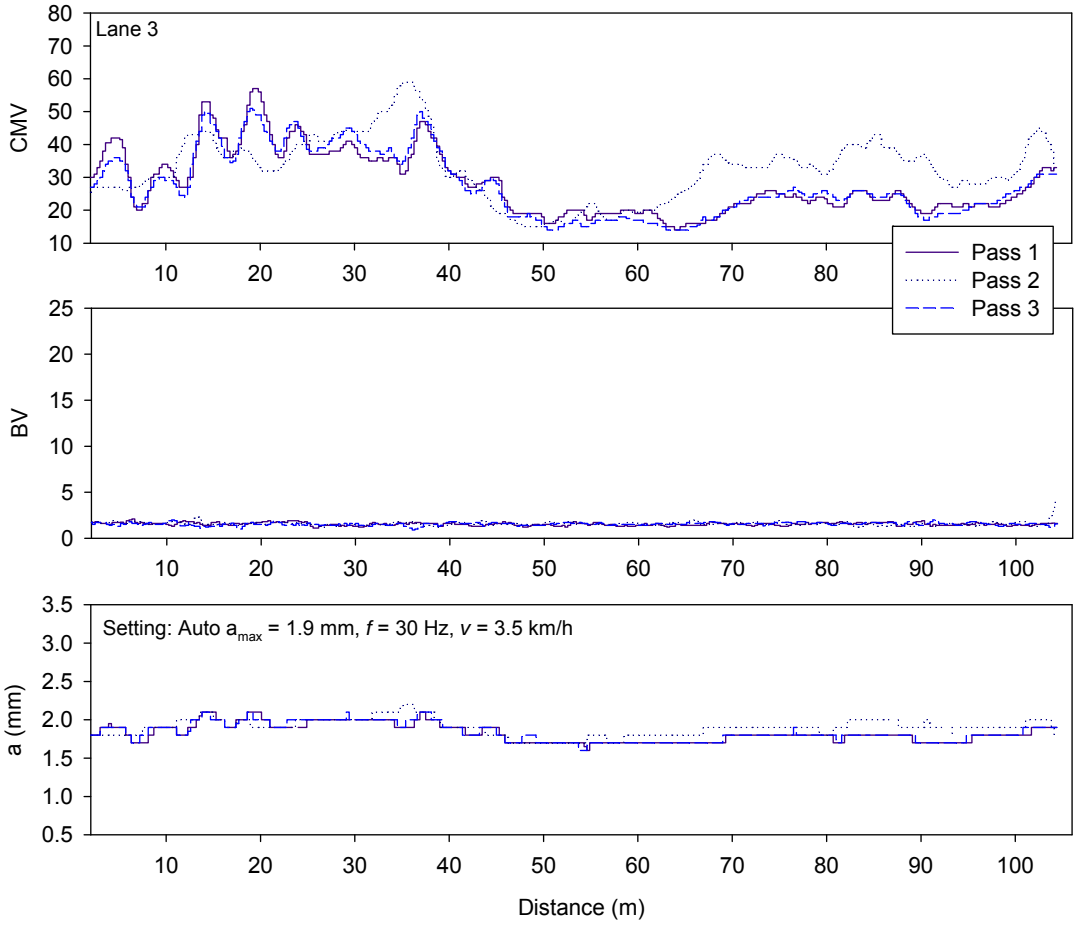

Figure 43. CMV and BV values for compaction passes on lane 3 of TB6 flex base material

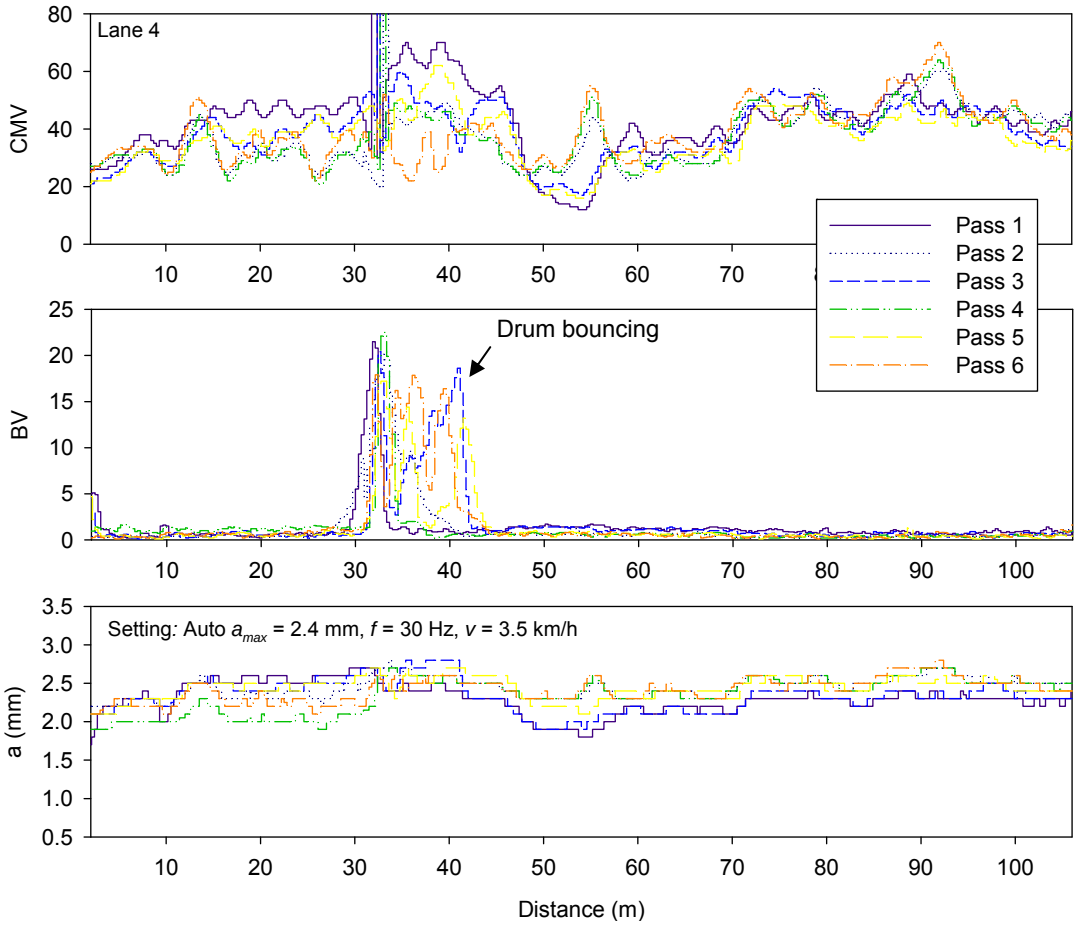

Figure 44. CMV, BV, and *a* values for compaction passes on lane 4 of TB6 flex base material

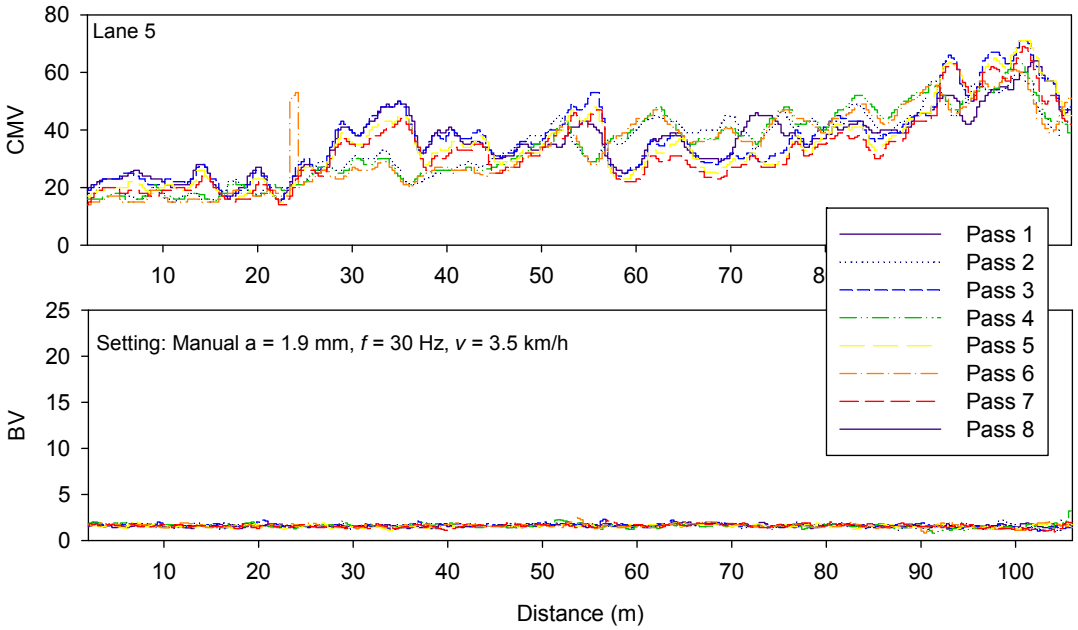

Figure 45. CMV and BV values for compaction passes on lane 5 of TB6 flex base material

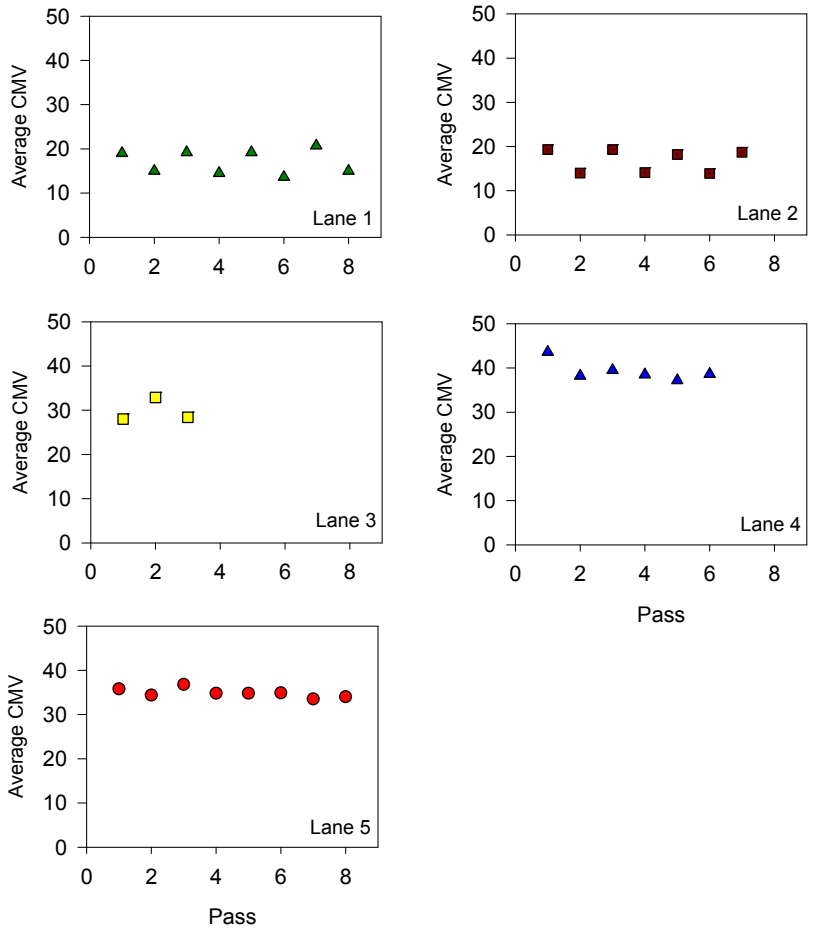

Figure 46. CMV compaction growth curves for TB 6 lanes 1 to 5

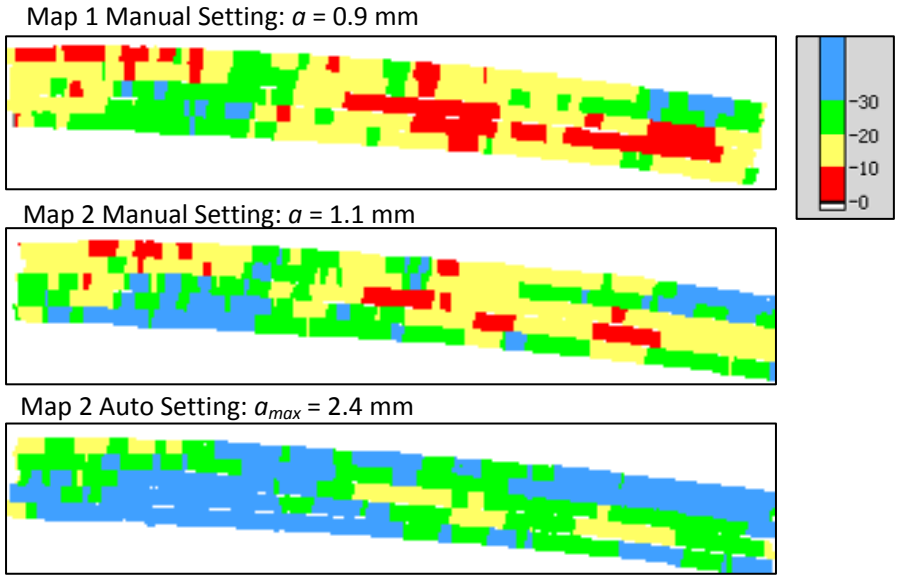

Figure 47. CMV maps on TB 7 with different operation settings

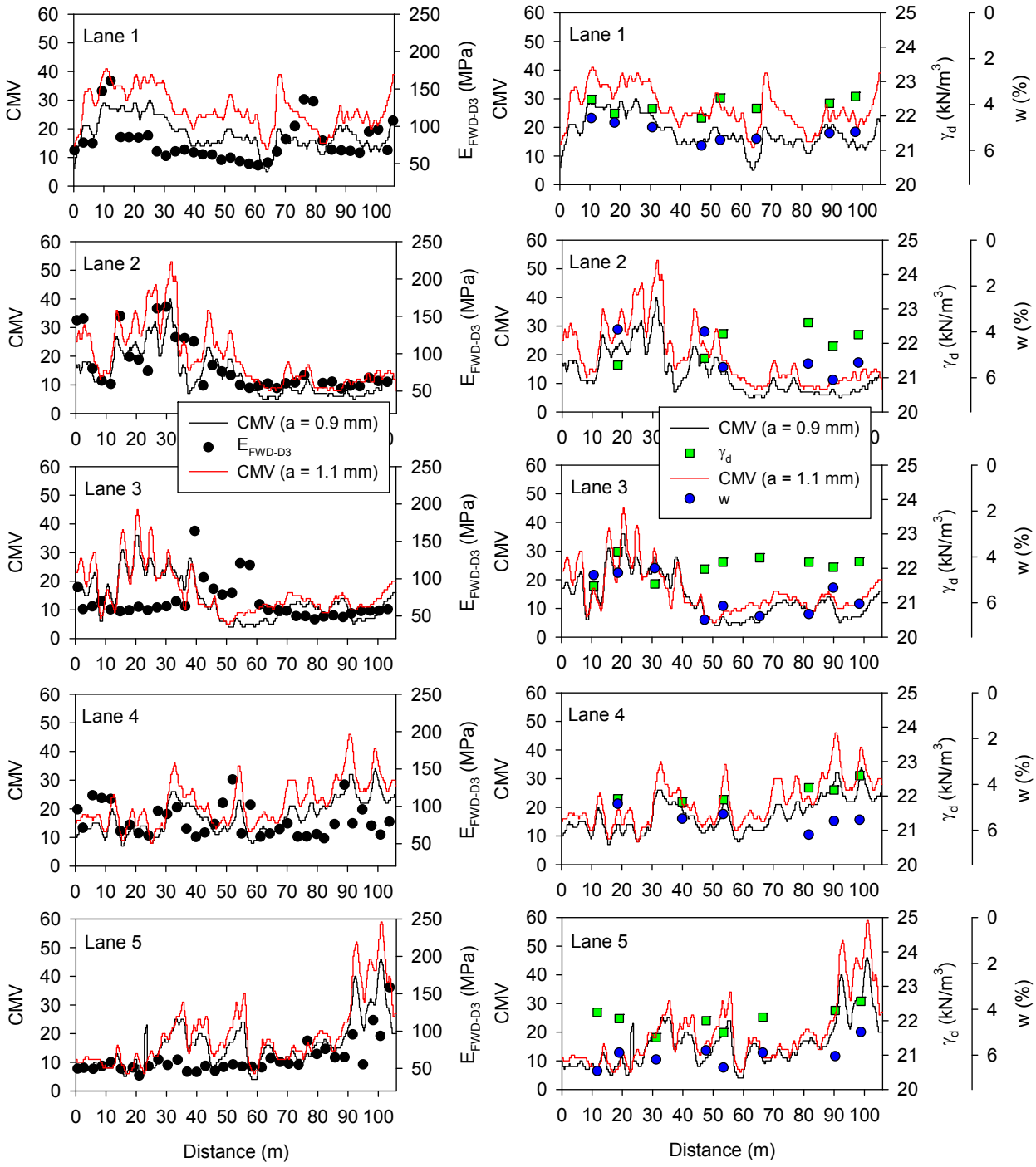

Figure 48. Comparison between CMV and in-situ point measurements (E_{FWD}, γ_d, and *w*) on TB 7 flex base material flex base material (nominal *f* = 30 Hz, *v* = 3.5 km/h)

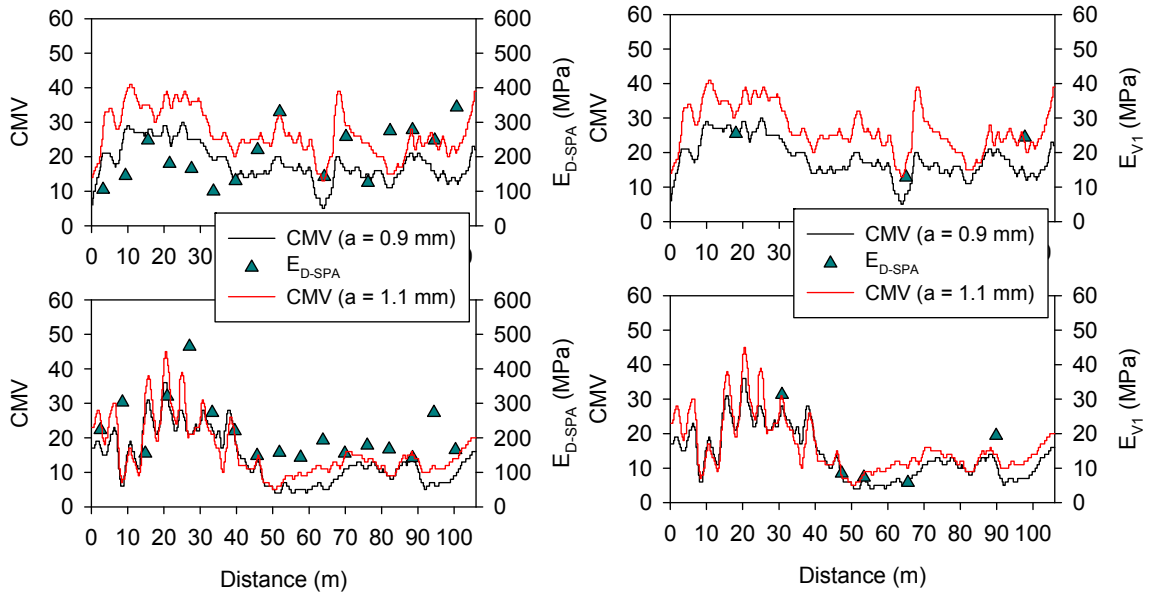

Figure 49. Comparison between CMV and point measurements (E_{D-SPA} and E_{V1}) on TB 7 flex base material flex base material (f = 30 Hz, v = 3.5 km/h)

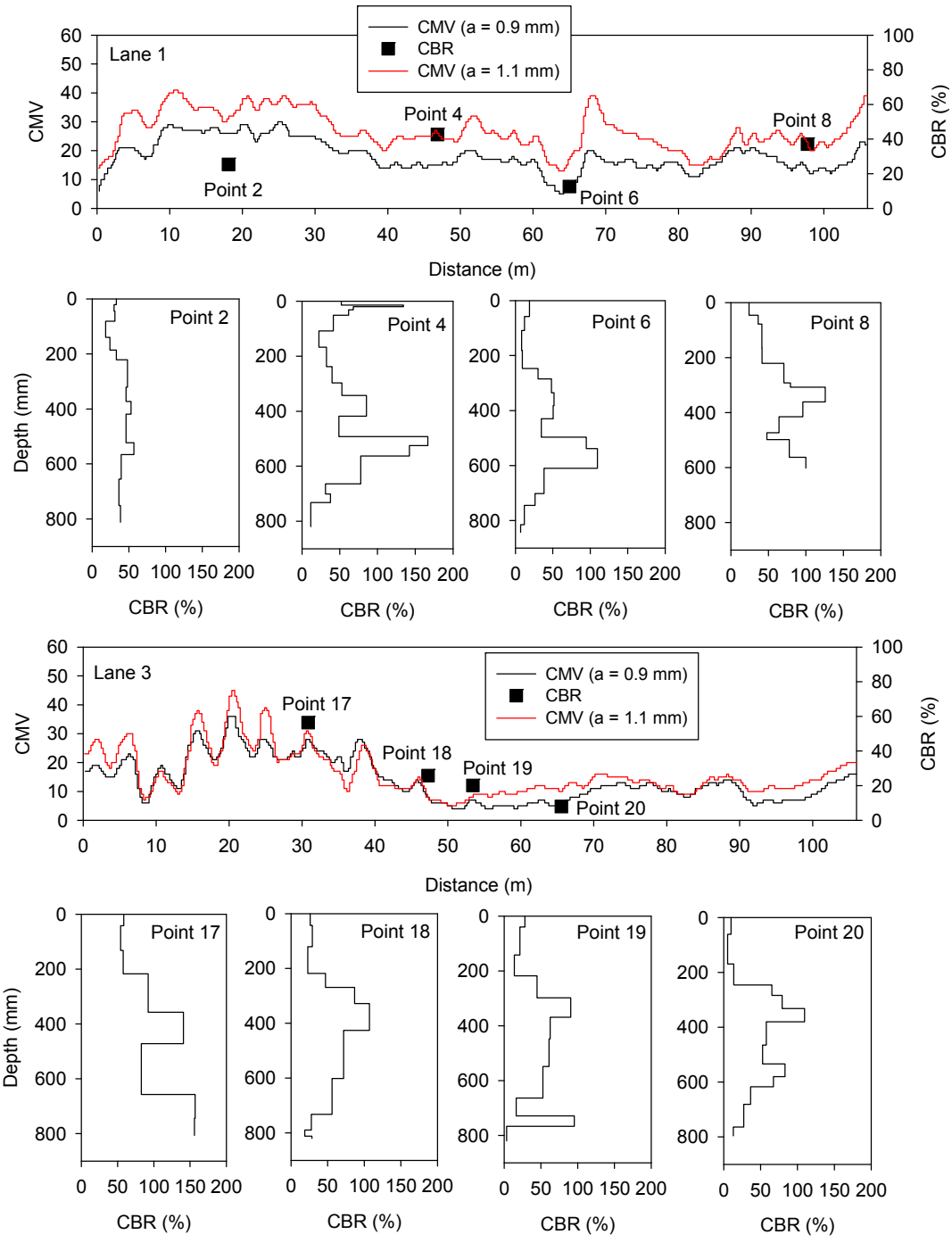

Figure 50. Comparison between CMV and DCP measurements on lanes 1 and 3 of TB 7 flex base material (nominal f = 30 Hz, v = 3.5 km/h)

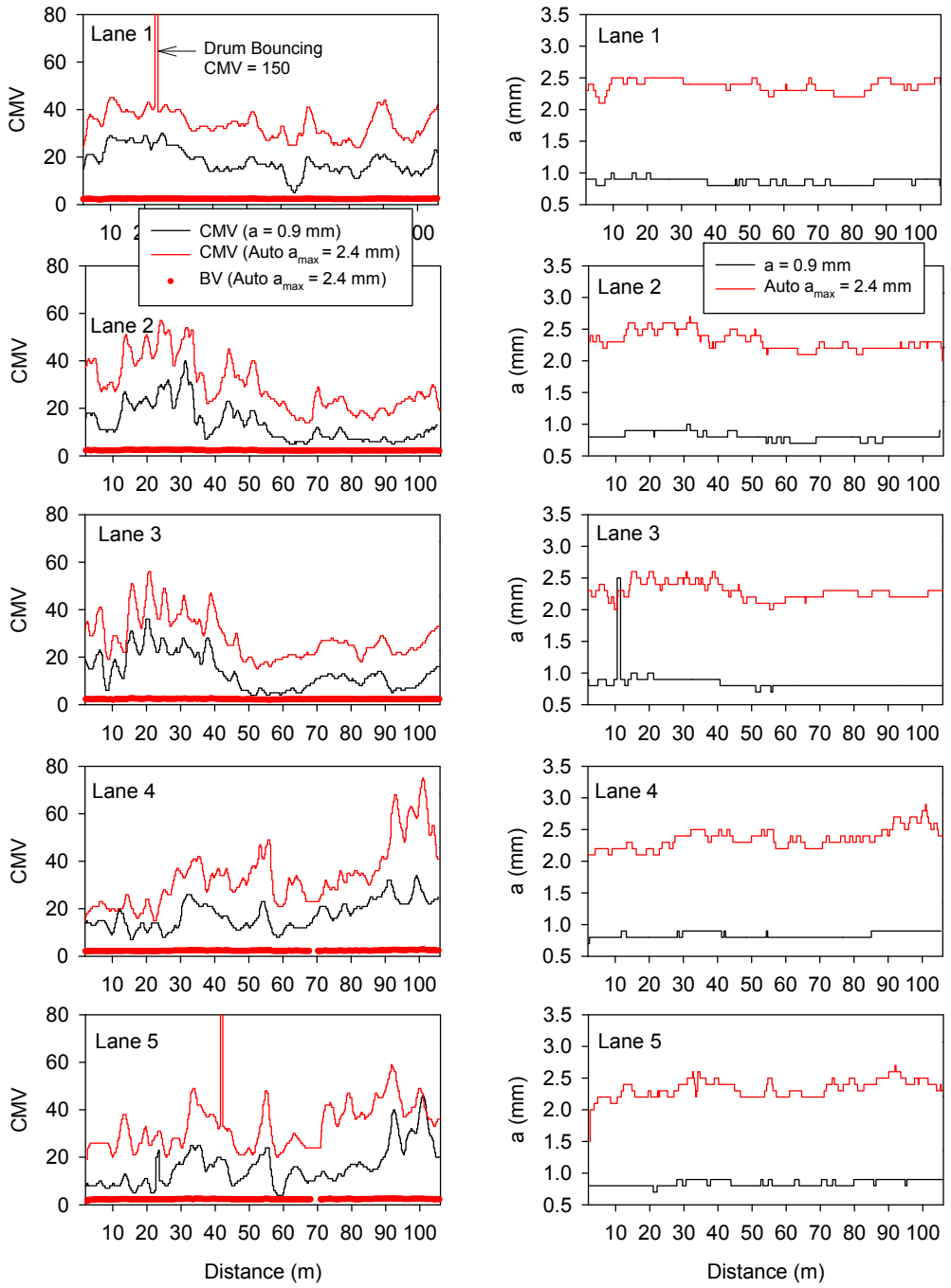

Figure 51. Comparison between CMV measurements in manual and automatic settings (nominal *f* = 30 Hz, *v* = 3.5 km/h)

Spatial analysis of roller-integrated and in-situ compaction measurements

Roller-integrated compaction measurements provide an opportunity to spatially visualize and quantify "non-uniformity" of compaction measurement values. This topic is slowly gaining popularity among the pavement engineering community. Vennapusa and White (2008) demonstrated the use of semivariogram analysis in combination with conventional statistical analysis to effectively address the issue of non-uniformity in quality assurance during earthwork construction. A variogram is a plot of the average squared differences between data values as a function of separation distance, and is a common tool used in geostatistical studies to describe spatial variation. Three important features of a semivariogram include: sill, range, and nugget. Sill is defined as the plateau that the semivariogram reaches, range is defined as the distance at which the semivariogram reaches the sill, and nugget is defined as the vertical height of the discontinuity at the origin which mostly represents sampling error or short scale variations (Srivastava, 1996). From a semivariogram model, a low "sill" and longer "range of influence" can represent best conditions for uniformity, while the opposite represents an increasingly non-uniform condition. Using these semivariogram parameters, theoretical models can be fit to the experimental semivariogram data. In the author's experience, exponential model generally fits well with the roller-integrated and in-situ compaction measurements (see White et al. 2007a, White et al. 2007b, Vennapusa and White 2008). Detailed descriptions of theoretical models can be found elsewhere in the literature (e.g., Clark and Harper 2002).

To evaluate the application of spatial analysis, spatially referenced CMV and E_{FWD} measurements obtained from TB 7 were analyzed. The comparisons are shown using theoretical and experimental semivariogram models, and Kriged surface maps generated for CMV and E_{FWD} measurements using the theoretical (exponential) semivariogram model. The theoretical semivariograms were fit to the experimental semivariograms by checking for its "goodness" using the modified Cressie goodness of fit approach suggested by Clark and Harper (2002) as well as the cross-validation process. A lower Cressie "goodness" factor and high R^2 value in cross-validation process indicates a better fit (see White et al. 2007a for additional details on model fitting process).

The semivariograms of CMV for two different amplitude settings showed similar effective ranges (6 m) but with higher sill for a = 1.1 mm than for a = 0.9 mm. This means that CMV data obtained with a = 1.1 mm setting was relatively more non-uniform than obtained with a = 0.9 mm. Univariate statistics (mean μ, standard deviation σ, and coefficient of variation COV) presented on Figure 52 show that the CMV from a = 1.1 mm setting was slightly higher on average than the CMV from a = 0.9 mm but with similar COV, however. This demonstrates the advantage of using spatial statistics for a better characterization of non-uniform conditions than using univariate statistics. The reasons for a difference in sill values of CMV for different amplitude settings are attributed to the materials' response to different stress conditions and possibly different influence depths. Increasing amplitude increases the contact stresses under the roller drum and also believed to increase the depth of influence under the drum. The E_{FWD} measurements showed slightly lower spatial continuity compared to CMV measurements with an effective range of about 4.5 m. The CMV and E_{FWD} Kriged contour maps are spatially comparable and showed similar spatial structure in their respective semivariograms.

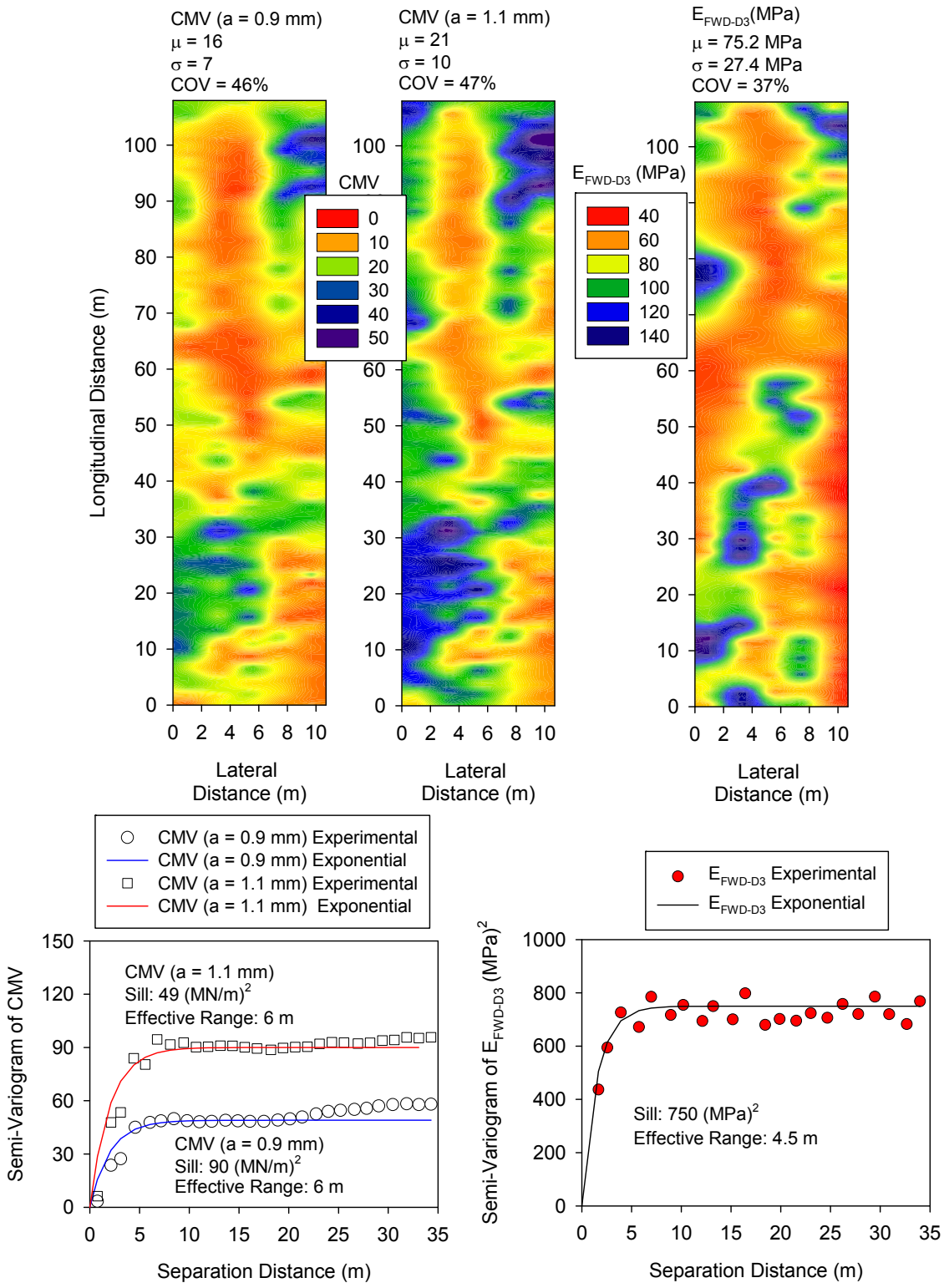

Figure 52. Kriged contour maps and semi-variograms of CMV and E_{FWD} on TB 7 flex base material

Summary

The roller-integrated CMV measurements showed good repeatability on the flex base material. Results from compaction passes did not show considerable increase in compaction with increasing passes. In some areas, the material was wet and "spongy" during compaction passes. The CMV measurements obtained from this test bed were in the range of 20 and 70. The CMV measurements on TB2 flex base material which was very dry were greater than about 100. This indicates that the material gains significant strength over time as the material is subjected to several days of compaction under construction equipment and as it becomes drier.

The CMV measurements are influenced by the vibration amplitude and show that increasing amplitude generally causes an increase in CMV on this material. Comparison between CMV and E_{FWD} measurements showed that the point measurements tracked well with the variability in CMV in some cases and in some cases it did not. The CMV measurements however were well correlated with variations in moisture content (within 4% to 6%) as evidenced by a decrease in CMV with increasing moisture content. $E_{D\text{-}SPA}$, E_{V1}, and CBR tracked well with the variations in CMV measurements. The reason for poorer correlation with E_{FWD} measurements in some locations is attributed to the possible influence of heterogeneity observed in the material across the drum width due to moisture segregation. Only one point measurement was obtained at the center of the drum while the roller value is an integrated response over the full drum width.

Spatial analysis was performed on CMV and E_{FWD} measurements to produce semivariograms and Kriged contour maps of the measurements. The CMV and E_{FWD} measurements are spatially comparable and showed similar spatial structure in their respective semivariograms. Spatial statistics (sill value) revealed high variability for CMV measurements obtained at a = 1.1 mm than CMV measurements obtained at a = 0.9 mm, which was not identified with univariate statistics (COV). This demonstrates that two data sets with identical distributions (i.e., same COV) can have significantly different spatial characteristics. Spatial statistics can provide a better characterization of "non-uniformity" than using univariate statistics.

Comparison between padfoot and smooth drum measurements – TBs 1, 3, 4, and 5

Comparison between k_{SlSD} and k_{SlPD} measurements obtained from TBs 1, 3, 4, and 5 are presented in Figure 553 to Figure 54. Although the results are slightly different in magnitude they show similar trends in variability. A regression relationship between k_{SlSD} and k_{SlPD} cannot be developed using the actual reported data since the values are not reported to exactly the same spatial location for each pass. To overcome this problem, the output data is processed in such a way that averaged data is assigned to a preset grid point along the roller path. Each grid point was spaced at approximately 0.5 m along the roller path which represents an average of measurements that fall within a window of size 0.25 m in forward and backward directions. Figure 56 shows linear regression relationship between k_{SlSD} and k_{SlPD} values using these averaged values and indicate that the two values are strongly correlated. Results show that k_{SlPD} values are generally greater than k_{SlSD}. Note that the values were obtained at different amplitude settings. Future studies may focus on obtaining correlations from the two measurements at similar amplitude settings. Anderegg (2008) indicated that the variation between k_{SlPD} and k_{SlSD} is a function of how deep the padfoot is penetrated into the ground. Comparison padfoot

penetration depth measurements in conjunction with k_{SISD} and k_{SIPD} measurements in future studies may help provide additional insights into the correlations between k_{SIPD} and k_{SISD} values. Nevertheless, the trends observed between k_{SIPD} and k_{SISD} are encouraging and the padfoot roller measurements demonstrate similar advantages as the smooth drum roller measurements.

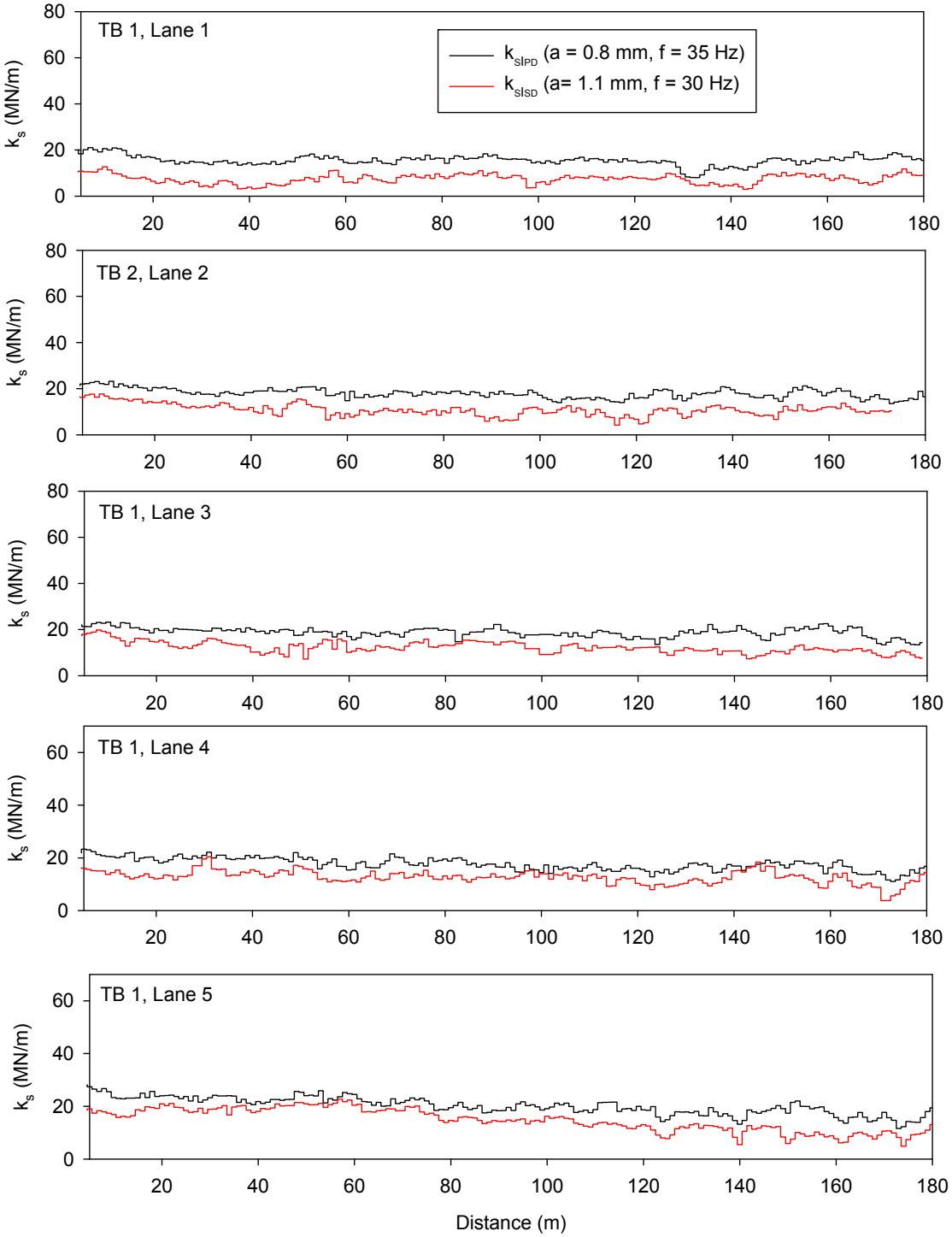

Figure 53. Comparison between k_{SIPD} and k_{SISD} measurements (TB 1 – subgrade clay material)

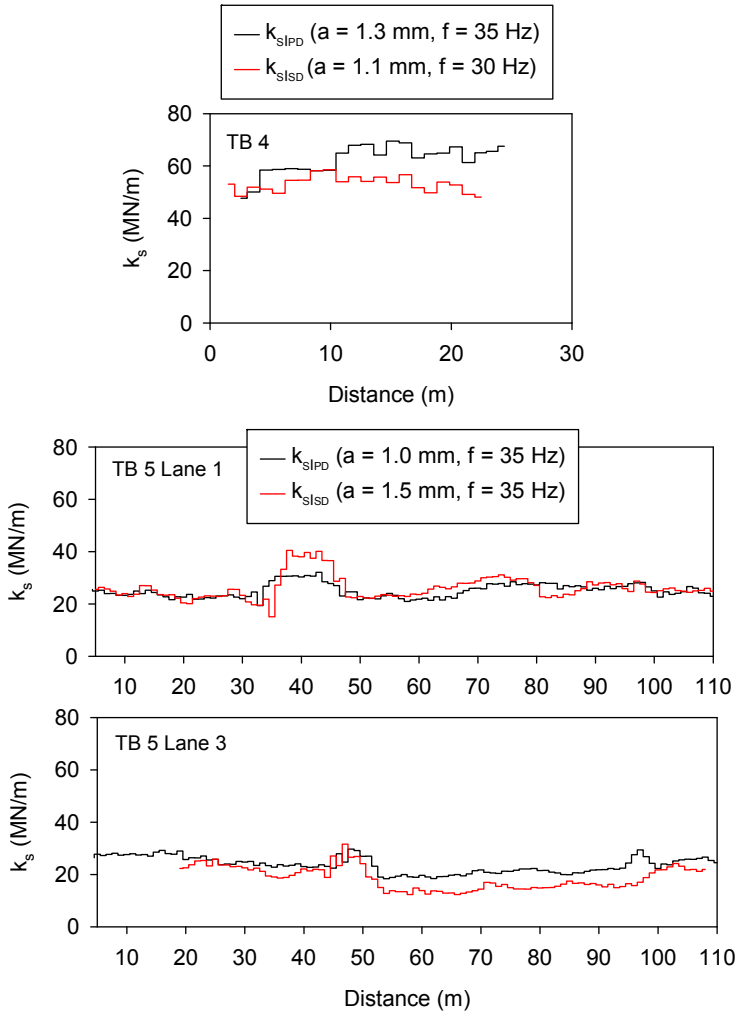

Figure 54. Comparison between k_{SIPD} and k_{SISD} measurements (TB 4 – flex base material and TB 5 – lime stabilized subgrade material)

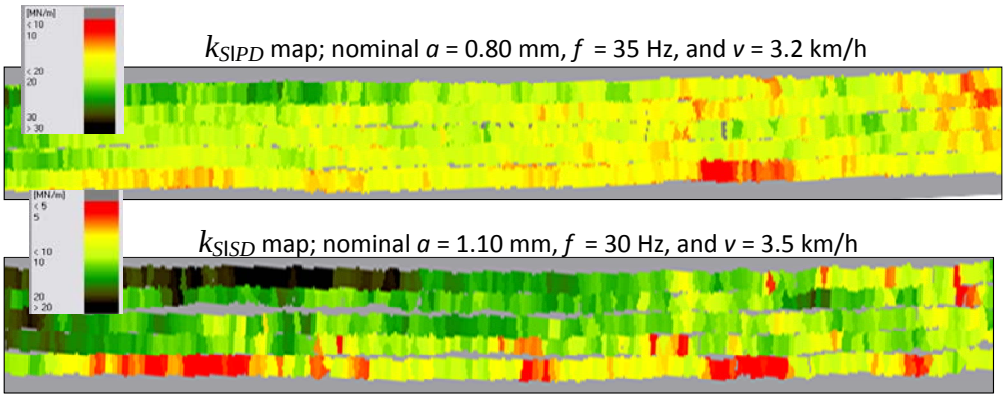

Figure 55. Spatial comparison of k_{SIPD} and k_{SISD} maps (TB 1 – subgrade clay material)

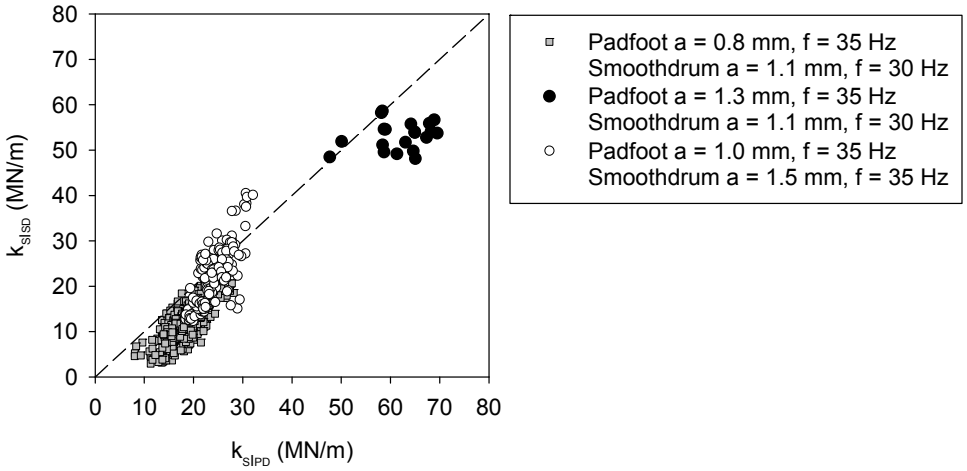

Figure 56. Relationship between k_{SlPD} and k_{SlSD} measurements

FIELD DEMONSTRATION

An open house was conducted on 07/25/2008 as part of this field investigation and included dissemination of results from previous IC field studies and results from the current field study as part of a presentation. The Iowa State University geotechnical mobile lab and demonstration of the three IC rollers was conducted at the project location. About 15 people attended the open house including Texas DOT, contractor, and roller manufacturer personnel. The attendees operated the IC rollers and received hands-on-experience.

SUMMARY AND CONCLUSIONS

The key findings from this study are as follows (as stated in TB discussions):

- Both padfoot and smooth drum roller-integrated k_s values (k_{slPD} and k_{slSD}) reliably indicate the compaction quality of the subgrade clay material with good repeatability. Correlations with E_{FWD} and E_{V1} values (with $R^2 > 0.6$) produced better R^2 values compared to $E_{LWD\text{-}Z2}$, γ_d, and CBR (of the compaction layer) measurements. poorer correlations with $E_{LWD\text{-}Z2}$, γ_d, and CBR compaction layer values is attributed to the limitation of shallow measurement influence depth of these measurements ($\leq$ 250 mm). CBR profiles up to 1 m generated from DCP tests identified "soft" zones below the compaction layer which affected the k_s values. The E_{V1} and $E_{FWD\text{-}D3}$ are believed to have influence depths that extend below the compaction layer due to higher applied contact stresses at the surface.
- Both roller MVs and in-situ point measurements captured the wide variation in stiffness of the compacted lime stabilized and flex base materials. A box-culvert located beneath the lime stabilized subgrade was identified with high roller MVs in that location. Linear regression relationships generally indicate separate linear trends for the lime stabilized and flex base materials. E_{FWD} measurements produced better correlations than other point

measurements. Hyperbolic regression relationships were developed for E_{FWD} and $E_{D\text{-}SPA}$ measurements which showed strong correlations with k_s and CMV measurements but additional data is needed to validate the relationships. The CMV measurements at this location were highly repeatable.

- Both padfoot and smooth drum roller-integrated k_s values (k_{slPD} and k_{slSD}) reliably indicated the compaction quality of the lime stabilized subgrade clay material with good repeatability. The k_s measurements effectively identified poor backfill compaction conditions along the edge of a box culvert located in this test bed and the results were confirmed from CBR profiles. Regression relationships between k_s and different in-situ point measurements show positive correlations with varying degree of uncertainty in the correlations (as assessed by the R^2 values), however. Better correlations were observed with $E_{FWD,}$ E_{V1}, E_{V2}, and E_{LWD} values (with $R^2 > 0.5$) compared to $E_{D\text{-}SPA}$ and γ_d. Relationships with $E_{D\text{-}SPA}$ show encouraging trends in the data, however. The k_s values were sensitive to moisture content of the compaction layer material.
- The roller-integrated CMV measurements showed good repeatability on the flex base material. Results from compaction passes did not show considerable increase in compaction with increasing passes. In some areas, the material was wet and "spongy" during compaction passes. The CMV measurements obtained from this test bed were in the range of 20 and 70. The CMV measurements on TB2 flex base material which was very dry were greater than about 100. This indicates that the material gains significant strength over time as the material is subjected to several days of compaction under construction equipment and as it becomes drier.
- The CMV measurements are influenced by the vibration amplitude and show that increasing amplitude generally causes an increase in CMV on this material. Comparison between CMV and E_{FWD} measurements showed that the point measurements tracked well with the variability in CMV in some cases and in some cases it did not. The CMV measurements however were well correlated with variations in moisture content (within 4% to 6%) as evidenced by a decrease in CMV with increasing moisture content. $E_{D\text{-}SPA}$, E_{V1}, and CBR tracked well with the variations in CMV measurements. The reason for poorer correlation with E_{FWD} measurements in some locations is attributed to the possible influence of heterogeneity observed in the material across the drum width due to moisture segregation. Only one point measurement was obtained at the center of the drum while the roller value is an integrated response over the full drum width.
- Spatial analysis was performed on CMV and E_{FWD} measurements to produce semivariograms and Kriged contour maps of the measurements. The CMV and E_{FWD} measurements are spatially comparable and showed similar spatial structure in their respective semivariograms. Spatial statistics (sill value) revealed high variability for CMV measurements obtained at $a = 1.1$ mm than CMV measurements obtained at $a = 0.9$ mm, which was not identified with univariate statistics (COV). This demonstrates that two data sets with identical distributions (i.e., same COV) can have significantly different spatial characteristics. Spatial statistics can provide a better characterization of "non-uniformity" than using univariate statistics.
- Comparison between k_{SlSD} and k_{SlPD} show that k_{SlPD} values are generally greater than k_{SlSD}. Note that the values were obtained at different amplitude settings. Future studies may focus on obtaining correlations from the two measurements at similar amplitude settings. Comparison padfoot penetration depth measurements in conjunction with k_{SlSD}

and k_{SlPD} measurements in future studies may help provide additional insights into the correlations between k_{SlPD} and k_{SlSD} values. Nevertheless, the trends observed between k_{SlPD} and k_{SlSD} are encouraging and the padfoot roller measurements demonstrate similar advantages as the smooth drum roller measurements.

REFERENCES

Anderegg, R. (1998). *Nichtlineare Schwingungen bei dynamischen Bodenverdichtern.* Ph.D. Dissertation, Eidgenossische Technische Hochschule Zurich (in German).

Anderegg, R., and Kaufmann, K. (2004). "Intelligent compaction with vibratory rollers." *Transp. Res. Rec.*, 1868, Journal of the Transportation Research Board, Washington D.C., 124–134.

Anderegg, R. (2008). *Testing the PD-Shell Single Drum Roller SV 212ACE.* July 31 (unpublished report).

Clark, I., and Harper, W. (2002). Practical geostatistics 2000. 3rd reprint, Ecosse North America Llc, Columbus, Oh.

Nazarian, S., Baker, M.R., and Crain, K. (1993). *Fabrication and Testing of a Seismic Pavement Analyzer.* SHRP Report H-375. National Highway Research Council, Washington, D.C.

Srivastava, R. M. (1996). "Describing spatial variability using geostatistical analysis." Geostatistics for Environmental and Geotechnical Applications, ASTM STP 1283, R. M. Srivastava, S. Rouhani, M. V. Cromer, A. J. Desbarats, A. I. Johnson, eds., ASTM, West Conshohocken, Pa, 13–19.

Vennapusa, P., White, D.J. (2008b). "Geostatistical analysis for spatially referenced roller-integrated compaction measurements, *Journal of Geotechnical and Geoenvironmental Engineering*, ASCE (in review, submitted July 2008).

White, D.J, Thompson, M., Vennapusa, P. (2007a). *Field Validation of Intelligent Compaction Monitoring Technology for Unbound Materials*, Mn/DOT Report No. MN/RC 2007-10, Iowa State University, Ames, IA.

White, D. J., Thompson, M., Vennapusa, P. (2007b). *Field study of compaction monitoring systems – Tamping foot 825 and vibratory smooth drum CS-533E rollers.* Final Report, Center of Transportation Research and Education, Iowa State University, Ames, Ia.

White, D. J. (2008). *Report of the Workshop on Intelligent Compaction for Soils and HMA.* Earthworks Engineering Research Center – Iowa State University and Iowa Department of Transportation, Ames, Iowa, April 2-4.

Yoo, T., Selig. E. (1980). "New concepts of vibratory compaction of soil," *Proc. of Intl. Conf. on Compaction*, Vol. II, Paris, pp. 703–707.

Zorn, G. (2003). *Operating manual: Light drop-weight tester ZFG2000,* Zorn Stendal, Germany.

APPENDIX

Accelerated Implementation of IC Technology for Embankment Subgrade Soils, Aggregate Base, and Asphalt Pavement Materials

Iowa State University Research Team Field Testing, FM 156 Fort Worth, Texas

Test Beds # 1/3 (07/21/2008 to 07/22/2008)

Description: The test bed was constructed by scarifying the existing subgrade material to a depth of about 250 mm (10 inches) and compacted in five lanes where two lanes (Lanes 4 and 5) were used as calibration test strips and the rest was used for production compaction. Lane 5 was prepared with three target moisture sections with moisture contents varying from dry to wet of the materials' optimum moisture content. The *Case/Ammann* pad foot roller was used for compaction for passes 1 to 10 and smooth drum roller was used for mapping (passes 11 to 14). In-situ point measurements (w, γ_d, CBR, and E_{LWD}) were obtained after 1, 2, 4, and 8 roller passes. Some point locations along lanes 1 and 5 were selected for E_{FWD}, E_{V1}, and E_{V2} testing (denoted as TB3). The objectives of this test bed were to obtain correlations between padfoot roller MVs and in-situ soil properties, and compare padfoot and smooth drum roller MVs.

Machine settings: Passes 1 to 8 – f = 35 Hz, Ecc. = 33%, a ~ 0.8 mm; Pass 9 – f = 35 Hz, Ecc. = 41%, a ~ 0.95 mm; Pass 10 – f = 30 Hz, Ecc. = 67%, a ~ 1.3 mm; Mapping Pass 11 – f = 30 Hz, Ecc. = 66%, a ~ 2.0 mm; Pass 12 – f = 30 Hz, Ecc. = 33%, a ~ 1.1 mm; Passes 13 to 14 – f = 30 Hz, Ecc. = 90%, a ~ 2.0+ mm.

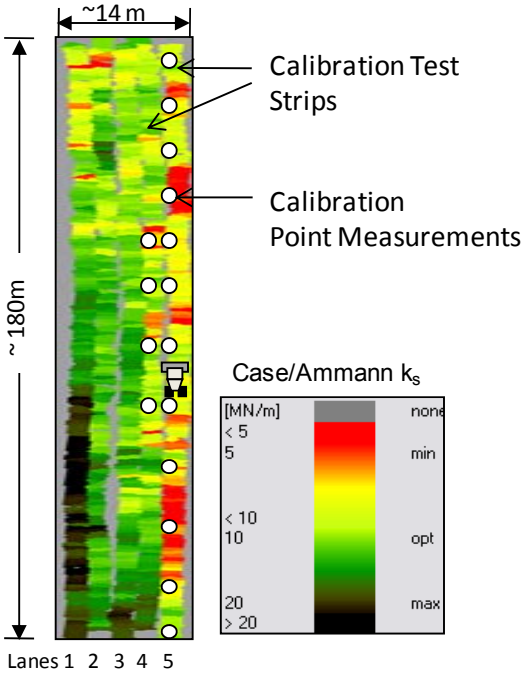

Construction/Testing Photos

Subgrade scarification using grader

Compaction using Case/Ammann padfoot roller

Zorn LWD

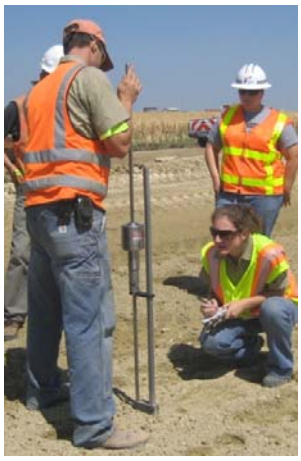

DCP

Accelerated Implementation of IC Technology for Embankment Subgrade Soils, Aggregate Base, and Asphalt Pavement Materials

Iowa State University Research Team Field Testing, FM 156 Fort Worth, Texas

Test Beds # 2/4 (07/22/2008)

Construction/Testing Photos

Description:

Test bed 2 consisted of a compacted layer of lime stabilized subgrade material transitioning to flex base at each end (see picture of the test bed). The flex base layer was significantly stiffer than the stabilized subgrade material. Case/Ammann and Dynapac smooth drum rollers were used for mapping the test bed. Following mapping passes, in-situ point measurements (w, γ_d, CBR, E_{LWD}, E_{FWD}, and $E_{D\text{-}SPA}$) were obtained from one lane of the test bed. The objectives of this test bed were to obtain measurements over a wide range of stiffness values for correlations with the two roller MVs.

Test bed 4 consisted of very stiff compacted flex base layer (see figure below). The TB was compacted using Case/Ammann padfoot roller to compare with smooth drum roller measurements.

Machine settings:
Case/Ammann smooth drum – Map 1
f = 30 Hz, Ecc. = 20%, a ~ 0.8 mm.
Dynapac smooth drum – Map 2: a ~ 1.2 mm.
Dynapac smooth drum – Map 3: a ~ 1.9 mm.

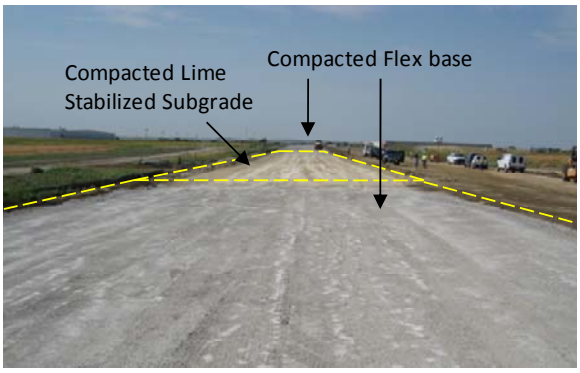

Picture of the testbed

FWD

D-SPA

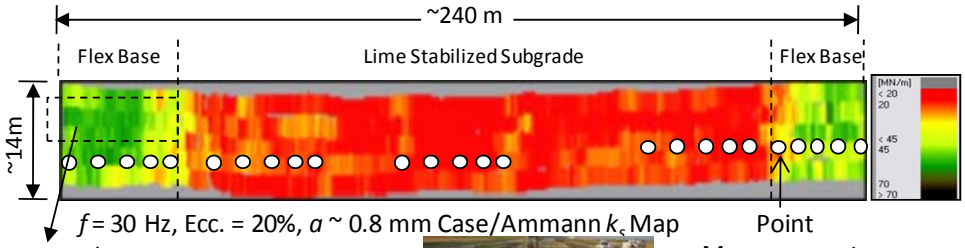

f = 30 Hz, Ecc. = 20%, a ~ 0.8 mm Case/Ammann k_s Map

Point Measurements

Test Bed # 4 (comparison between Case/Ammann padfoot roller and smooth drum roller)

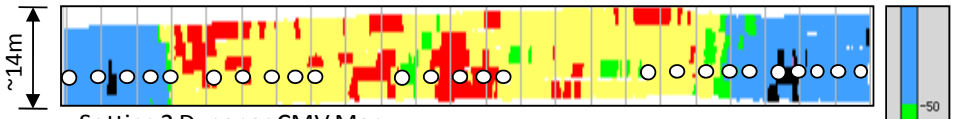

Setting 2 Dynapac CMV Map

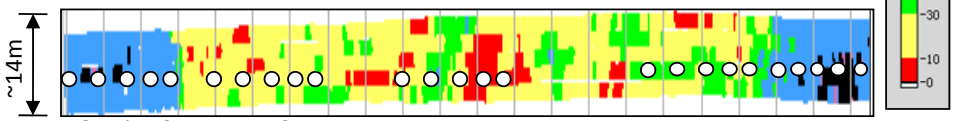

Setting 3 Dynapac CMV Map

Accelerated Implementation of IC Technology for Embankment Subgrade Soils, Aggregate Base, and Asphalt Pavement Materials

Iowa State University Research Team Field Testing, FM 156 Fort Worth, Texas

Test Bed # 5 (07/23/2008)

Description: The test bed consisted of lime-treated subgrade material. The material was reclaimed and moisture conditioned to a depth of about 250 mm. A concrete box culvert was located under a section of the TB with a transition between stiff material over the culvert and a small area of poorly compacted backfill along the edge of the culvert (see Figure below). The TB was compacted in six roller lanes with three lanes each using padfoot and smooth drum Case/Ammann rollers. One lane each was selected as calibration test strip for each roller and the remaining area was used for production compaction. In-situ point measurements (w, γ_d, CBR, and $E_{LWD\text{-}Z2}$) were obtained after 1, 2, 4, 8 and 12 roller passes on the calibration test strips. E_{FWD} and $E_{D\text{-}SPA}$ tests were conducted on one lane after production compaction. The objectives of this test bed were to obtain correlations between roller MVs and in-situ point measurements, evaluate the efficiency of the roller in identifying poorly compacted backfill areas around the culvert, compare padfoot and smooth drum compaction process on lime stabilized subgrade material.

Machine settings:
Lane 1 – Passes 1 to 8 *f* = 35 Hz, Ecc. = 50%.
Lane 2 – Passes 1 to 8 *f* = 30 Hz, Ecc. = 70%.
Lane 3 – Passes 1 to 12 *f* = 35 Hz, Ecc. = 35%.
Lane 4 – Passes 1 to 8 *f* = 35 Hz, Ecc. = 50%.
Lane 5 – Passes 1 to 6 *f* = 35 Hz, Ecc. = 33%.
Lane 6 – Passes 1 to 6 *f* = 35 Hz, Ecc. = 67%.
Map 1: *f* = 35 Hz, Ecc. = 50%
Map 2: *f* = 35 Hz, Ecc. = 33%
Map 3: *f* = 35 Hz, Ecc. = 20%

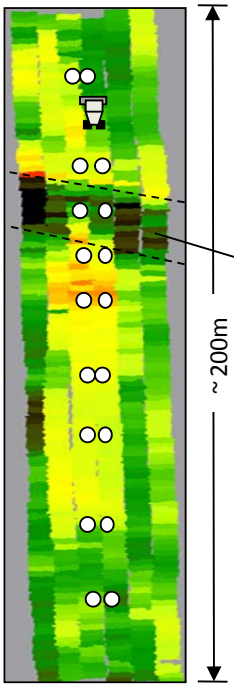

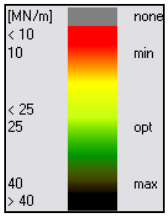

Lane 3 – padfoot calibration strip
Lane 4 – smooth drum calibration strip

Testing Photos

Point measurements on calibration strips

LWD

PLT

Box Culvert

Lanes 1 to 3 (from left) – padfoot
Lanes 4 to 6 (from left) – smooth drum

Accelerated Implementation of IC Technology for Embankment Subgrade Soils, Aggregate Base, and Asphalt Pavement Materials

Iowa State University Research Team Field Testing, FM 156 Fort Worth, Texas

Test Bed # 5 (07/23/2008) Construction Photos

Accelerated Implementation of IC Technology for Embankment Subgrade Soils, Aggregate Base, and Asphalt Pavement Materials

Iowa State University Research Team Field Testing, FM 156 Fort Worth, Texas

Test Beds # 6 (07/23/2008)

Description: TB6 consisted of flex base material placed and graded to the project grade. The layer was moisture conditioned and then compacted using Dynapac smooth drum roller in five roller lanes. Compaction was performed in different machine settings (see below) for each lane. Following compaction, the area was mapped using manual and automatic feedback control settings. The objectives of this test bed were to investigate differences for different machine settings.

Machine settings (compaction):
Lane 1: Manual setting, *a* = 0.9 mm
Lane 2: Manual setting, *a* = 1.1 mm
Lane 3: Auto setting, Maximum *a* = 1.9 mm
Lane 4: Auto setting, Maximum *a* = 2.4 mm
Lane 5: Manual setting, *a* = 1.9 mm

Machine settings (mapping):
Map 1: Manual setting, *a* = 1.2 mm
Map 2: Manual setting, *a* = 1.9 mm
Map 3: Auto setting, Maximum *a* = 2.4 mm

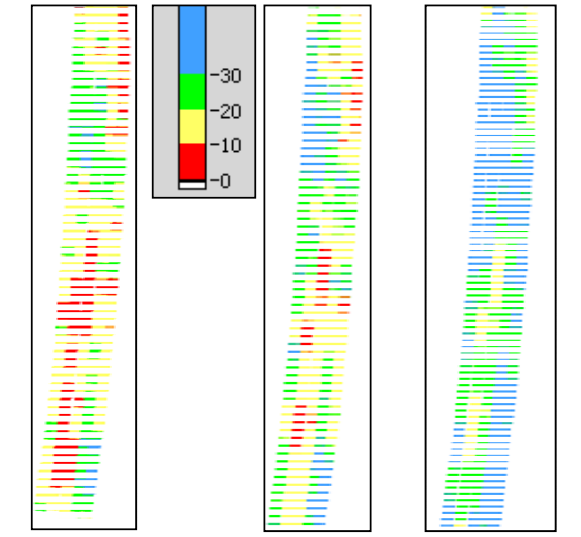

Map 1 Manual Setting 2 *a* = 0.9 mm

Map 2 Manual Setting 3 *a* = 1.1 mm

Map 3 Auto Setting 5 *a(max)* = 2.4 mm

Construction Photos

Accelerated Implementation of IC Technology for Embankment Subgrade Soils, Aggregate Base, and Asphalt Pavement Materials

Iowa State University Research Team Field Testing, FM 156 Fort Worth, Texas

Test Beds # 7 (07/23/2008)

Testing Photos

Description: TB7 involved performing in-situ point measurements on compacted TB6 flex base material. Point measurements included w, γ_d, CBR, E_{LWD-Z2}, E_{FWD-D3}, E_{V1}, E_{V2}, and E_{D-SPA}. The objectives of this TB were to obtain comparison soil property measurements to roller MVs and develop contour maps of soil properties to spatially compare with roller MVs.

Point measurements:

Plate load tests : 9 locations
Nuclear gauge tests: 37 locations
DCP tests: 11 locations
FWD tests: 175 locations
D-SPA tests: 33 locations